POLITECNICO DI TORINO

Department of Electronics and Telecommunications
Master's Degree in Electronic Engineering

Master's Thesis

Analysis of Passive Intermodulation in a Junction: Physical Simulation Models for Non-Linear Electrical Contacts

Supervisors:
Prof. Flavio Canavero
Prof. Riccardo Trinchero

Candidate:
Enrico Sapienza

Academic Year 2018-2019

Summary

Passive intermodulation (PIM) is a growing issue in several communication systems, like cellular networks, shipboard systems and satellite communication systems. These intermodulation products are due to the non linear behaviour of passive components in which the signals travel. But, unlike the more known distortions due to active devices, they are more complicated to remove and can lead to problems during the communication. Indeed, these unwanted frequencies can fall within the receiver band, leading to interference problems and reducing the performance of the whole system. Specifically, the arise of PIM is related to the non ideal metal-metal (MM) contacts in the system. The goal of this thesis is to develop an equivalent circuit model able to describe the behaviour of a MM joint. In order to do this, two different approaches have been considered: a physical-based model and a behavioural-based one. A physical-based approach allows to develop a general model for the contact based on mathematical equations. But, such a model is difficult to develop due to the different microscopic effects which influence such a junction and the several parameters that should be accurately estimated. On the other hand, the behavioural-based approach allows to overcome the above issues, thus providing a reliable modeling scheme. Several experimental setups and measurement configurations have been considered. Among them, the setup based on a steel-copper contact provides the most stable configuration. Thanks to a spectrum analyzer, we were able to observe PIM and, analyzing the chosen setup, it was possible to develop a model able to fully characterize the behaviour of the above contact. Furthermore, the model was validated by comparing the experimental results with the ones predicted by the proposed behavioural-based model via simulations through a full-wave solver (e.g. *CST Microwave Studio*).

Acknowledgments

Vorrei ringraziare il prof. Canavero e il prof. Trinchero, relatori di questa tesi di laurea, per l'aiuto fornitomi e per la disponibilitá dimostratami durante tutto il periodo di stesura.
Un grande ringraziamento a mia madre, mio padre, mia sorella, i miei nonni e tutta la mia famiglia per il loro immancabile sostegno morale ed economico e per il loro affetto, prezioso per giungere a questo punto.
Un grazie speciale a Marilena, che mi é stata sempre vicina e mi ha sostenuto nei momenti difficili di questi anni.
Vorrei inoltre ringraziare Saro e Serena, i miei amici di una vita, con i quali ho condiviso momenti belli e brutti di questo percorso e che in diverse occasioni hanno saputo darmi consigli e suggerimenti preziosi.
Ci tengo a ringraziare anche Dario, la prima persona conosciuta in questa mia nuova avventura, che mi é stato sempre vicino non facendomi mai mancare il suo supporto.
Un grazie anche ai miei amici di Catania, i quali, anche se distanti parecchi kilometri, non mi hanno mai fatto mancare il loro sostegno e il loro affetto.
Infine, vorrei ringraziare i miei amici del collegio, con i quali ho trascorso momenti indimenticabili che porteró sempre con me.

Table of contents

List of figures

Chapter 1

Introduction

In communication systems, like cellular networks, deep space probe networks, shipboard systems and satellite communication systems, in which there are transmitter and receiver units that operate simultaneously, any generated intermodulation frequencies (IM) that fall within the local receiver band can lead to several problems, reducing the performance of the system [1]. For this reason, the study of these intermodulation frequencies is very important, in order to understand why they appear and try to reduce them as much as possible. The most known intermodulations are due to active devices, whose non linear characteristic is source of distortion. But not only active devices lead to distortion, also passive devices can introduce non linear effects. In this case, we are talking about *passive intermodulation* (PIM), highlighting that these intermodulations are due to passive devices. Although sometimes they are relatively small, these intermodulations can have serious effects on system performance.

1.1 PIM frequencies

In order to understand the generation of passive intermodulation frequencies, we consider a passive device which is excited, for sake of simplicity, by two signals with frequencies f_1 and f_2:

$$V = V_1 sin(2\pi f_1 t) + V_2 sin(2\pi f_2 t) \tag{1.1}$$

where V_1 and V_2 are the amplitudes of input signals. Intermodulation frequencies are given by:

$$f_{int} = mf_1 \pm nf_2 \tag{1.2}$$

where f_{int} is the frequency of intermodulation product, m and n are integer numbers. The order of intermodulation product N is given by the following relation:

$$N = m + n \tag{1.3}$$

In Fig.(1.1) is reported an example which shows the presence of two carrier frequencies f_1 and f_2 and the resulting intermodulation products of 3^{rd}, 5^{th} and 7^{th} order.

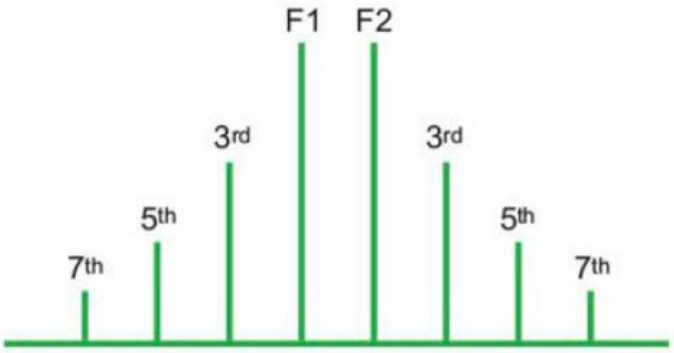

Figure 1.1. Passive intermodulation frequencies of 3^{rd}, 5^{th} and 7^{th} order

These new frequencies originated by transmitter can fall in the reception band, as shown in Fig.(1.2).

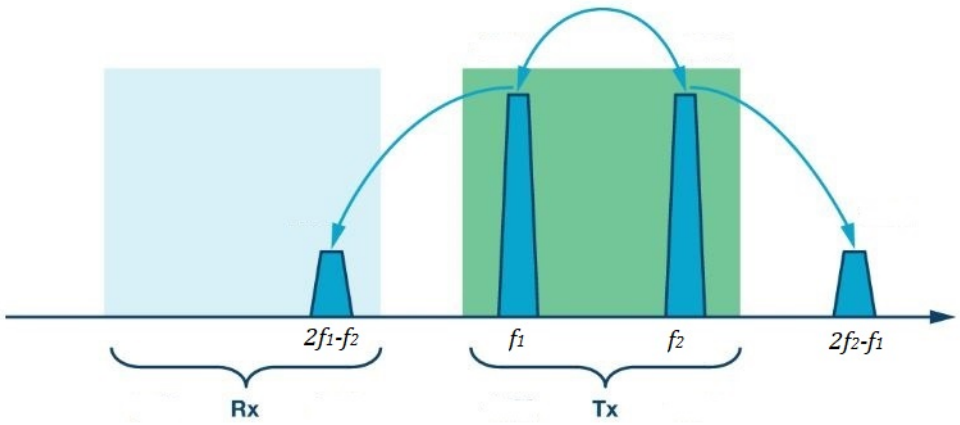

Figure 1.2. Passive intermodulation frequency falling into the receiver band

Despite the fact that these intermodulation products have low power, if they fall into the frequency band of the receivers, interference problems can occur, reducing the receiver sensitivity or may even inhibit communication completely. In fact, passive intermodulation frequencies cannot be filtered out and, for this reason, they could be more dangerous than intermodulation products due to active components. It is for this reason that passive intermodulation is a significant issue within the mobile phone industry.

1.2 PIM sources

These intermodulation products are the result of two or more input signals travelling through passive devices like contacts, waveguide junctions, coaxial connectors, antennas. The distortion can be related to the presence of these nonlinear components, which generate harmonics of the input signal [2]. If we suppose to excite a non linear system with a sinusoidal signal of frequency ω_0, looking at the output signal spectrum, in addition to the fundamental frequency component, we can notice the presence of components at frequencies which are multiples of the fundamental one ($2\omega_0$, $3\omega_0$,...):

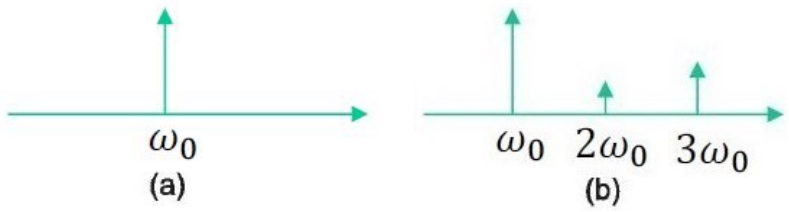

Figure 1.3. a) Spectrum of input signal b) Spectrum of output signal

In a communication system, we can manly distinguish between two types of passive nonlinearities:

- Material nonlinearity
- Contact nonlinearity

The first one is intrinsically related to the material used. In fact, some materials, such as ferromagnetic ones, exhibit nonlinear electrical characteristics. The second one is related to the imperfection of metal contacts, which have nonlinear current voltage characteristic. This nonlinear behaviour is due to the roughness of contact surfaces and to the presence of a dielectric layer between them. In fact, all metal

surfaces, except gold, always show a native oxide or sulfide layer covering them. The thickness of this layer depends on the metal itself, but generally is not thicker than few nanometers. An example of contact between two rectangular waveguide flanges is shown in Fig.(1.4), [9].

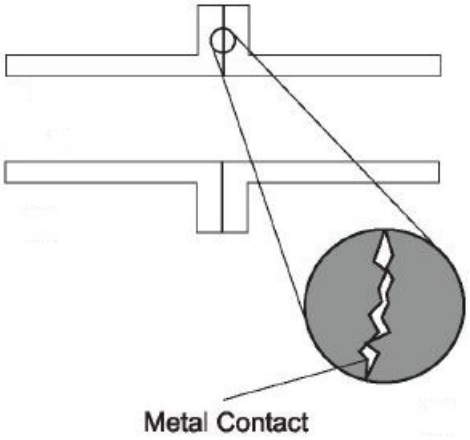

Figure 1.4. Cross sectional view of the contact between two rectangular waveguide flanges

As we can see, the contact is not perfect due to the presence of a dielectric layer and air gaps between the flanges. The physical mechanisms which underlie the non-linear effects are complex and not very understood. Along the years, from the first investigation to today, several mechanisms have been identified as the main source of passive intermodulation. Considering a metal contact, like the one reported in Fig.(1.4), according to solid physics theory, the possible PIM sources are tunnel current through the oxide layer, constriction resistances, non linear conductivity and electro-thermal processes like thermionic emission, Poole-Frenkel effect and temperature dependent conductivity [2][3]. The main problem is that these sources are difficult to isolate experimentally and, hence, the comparison between theory and experimental data it's really hard.

Chapter 2

Equivalent circuit model of contact between two metals

2.1 Contact model of rough surfaces

The goal of this thesis is to develop a circuit model which is able to characterize the behaviour of a metal-metal contact. This equivalent circuit, in order to take into account all effects due to the non perfect contact, should be a combination of linear dynamic elements (capacitors and inductors) and static ones (resistors) with a non linear one, that is the real source of PIM frequencies, represented by a non linear resistance, as schematically shown in Fig.(2.1).

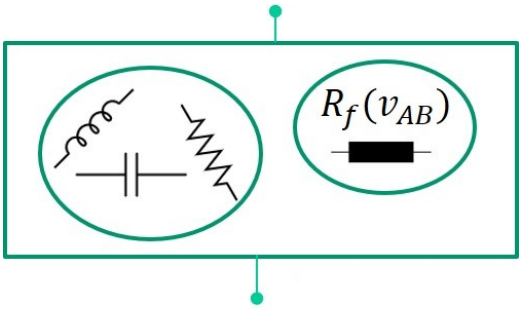

Figure 2.1. Linear and non linear elements of circuital model

In order to develop this model, two different approaches have been considered in this work:

- Physical-based modeling
- Behavioural-based modeling

The first approach allows to provide a general equivalent circuit in which the circuit parameters are estimated via mathematical equations, while, in the second one, they are estimated starting from experimental data obtained from measurements carried out in laboratory.

Chapter 3

Physical-based model

The first considered approach was the physical-based one. As explained before, usually waveguide metals react with air or other oxidizing agents and form a few nanometers oxide layer on the surface. Thus, in practice, instead of having a pure metal-metal contact (MM), we have a metal-insulator-metal contact (MIM). If this layer is thin enough (few tens of Ångström), some electrons can pass trough the oxide giving rise to a current.

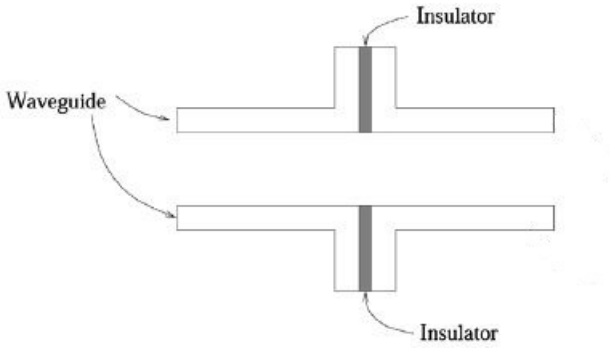

Figure 3.1. Oxide layer between two rectangular waveguide flanges

From the microscopic point of view, the contact between two metal surfaces is reported in Fig.(3.2).

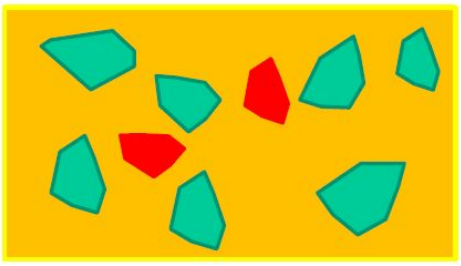

Figure 3.2. Microscopic view of a contact between two metal rough surfaces in which are shown MM contacts (green) and MIM contacts (red)

As we can note in Fig.(3.2), in the contact area we can distinguish two kinds of contacts: MM contacts (reported in green) and MIM contacts (in red). In order to understand better the parameters that we have to take into account in our analysis, a cross-section view of the contact is needed:

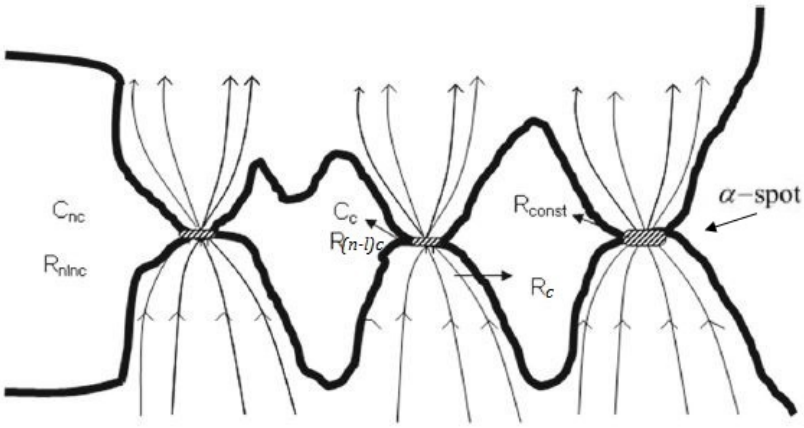

Figure 3.3. Microscopic cross-section of a contact between two metal rough surfaces

As we can see in the Fig.(3.3), due to the roughness of surfaces, there is the presence of two regions: contacting zones and non contacting ones. In the contacting points two situations can happen. If the pressure contact is high enough, the oxide film could break and the two metals are put in contact directly. In this case we have a MM contact which are called $\alpha-$spots. Instead, if the pressure of the contact is not enough to break the oxide film between the two surfaces, we have a MIM contact. It is clear that higher is the contact pressure, higher is the number of $\alpha-$spots. According to this microscopic view and taking into account all capacitive and resistive

effects, one of the most valuable equivalent circuit model present in literature is the one depicted in Fig.(3.4), [2].

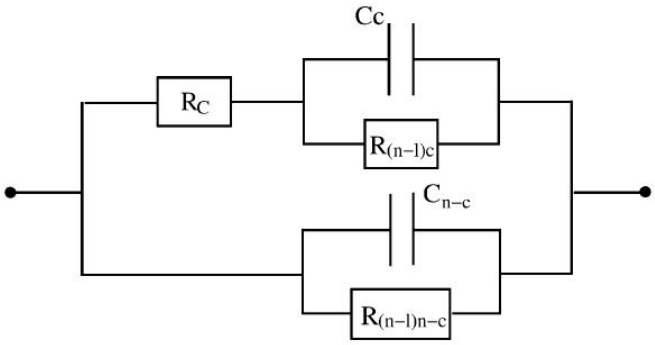

Figure 3.4. Equivalent circuit model of a contact junction if no $\alpha-$spots are present

As we can see in the picture, the equivalent circuit consists of two parallel branches: the upper one is needed to model the contacting zones, while the lower one is related to the void regions where there is no contact. In particular, this circuit is used in the case where the contact pressure is low and there is not the formation of $\alpha-$spots. The upper branch consists of a parallel connection between a capacitor (C_c) and a non linear resistor ($R_{(n-l)c}$), connected in series with a resistor (R_c). The contacting capacitance C_c is given by:

$$C_c = \frac{\epsilon_0 \epsilon_r A_n A^*}{s} \tag{3.1}$$

where ϵ_0 and ϵ_r are, respectively, the vacuum and the oxide permittivity, A_n the nominal contact area, s the oxide film thickness and A^* the dimensionless real area of contact defined as the ratio between the real contact area and the nominal one and given by:

$$A^* = \pi \beta l_c^* \left[\int_{d^*}^{d^*+l_c^*} K^1 + 0.93 \int_{d^*+l_c^*}^{d^*+6l_c^*} K^{1.136} + 0.94 \int_{d^*+6l_c^*}^{d^*+110l_c^*} K^{1.146} + 2 \int_{d^*+110l_c^*}^{\infty} K^1 \right] \tag{3.2}$$

where:

$$K^\beta = \left(\frac{l^*}{l_c^*} \right)^\beta \phi^*(z^*) dz^* \tag{3.3}$$

β is a parameter related to the surface called roughness parameter and it is given by:

$$\beta = \eta\sigma R \tag{3.4}$$

where η is the asperity density, σ is the standard deviation of the surface heights and R is the asperity radius. The parameter l_c is the critical interference, which is the index of transition from elastic deformation to the elastic-plastic one. It is related to the hardness of the softer material (H) according to the following equation:

$$l_c = \left(\frac{\pi K H}{2E'}\right)^2 R \tag{3.5}$$

where K is related to the Poisson's ratio ν of the softer material by:

$$K = 0.454 + 0.41\nu \tag{3.6}$$

E' is the Hertz elastic modulus and is given by:

$$\frac{1}{E'} = \frac{1-\nu_1^2}{E_1} + \frac{1-\nu_2^2}{E_2} \tag{3.7}$$

where E_1 and E_2 are the Young's moduli of the two metals and ν_1 and ν_2 their respective Poisson's ratios. $\phi^*(z^*)$ is the dimensionless asperity heights probability density function given by:

$$\phi^*(z^*) = \frac{1}{\sqrt{2\pi}}\frac{\sigma}{\sigma_s}\exp\left[-0.5\left(\frac{\sigma}{\sigma_s}\right)^2 (z^*)^2\right] \tag{3.8}$$

where σ_s is the standard deviation of the asperity heights, which is related to σ by:

$$\frac{\sigma_s}{\sigma} = \sqrt{1 - \frac{3.717\cdot 10^{-4}}{\beta^2}} \tag{3.9}$$

The resistance R_c is called constriction resistance and it is introduced to model the sharp contraction of the current in the asperity regions. For a single microasperity, the constriction resistance is given by:

$$R_{c_i} = \frac{\rho_1 + \rho_2}{4R} \tag{3.10}$$

where ρ_1 and ρ_2 are the resistivities of the contacting surfaces. For N_c microasperities in contact, the total constriction resistance R_c is given by the parallel of all single resistances:

$$R_c = \frac{\rho_1 + \rho_2}{4N_c\bar{R}} \tag{3.11}$$

where $\bar{R}$ is an average radius given by:

$$\bar{R} = \sqrt{\frac{A_n A^*}{\pi N_c}} \tag{3.12}$$

The last and most important element in the upper branch is the non linear resistor $R_{(n-l)c}$. This resistance is due to the presence of the oxide layer and, together with the non linear one present in the lower branch, it represents the PIM source. The lower branch consists only of a non linear resistor ($R_{(n-l)n-c}$) connected in parallel with a capacitor (C_{n-c}). This capacitance is due to the void regions between the metal surfaces and it is the sum of two contributions: the air capacitance of thickness $d - s$, where d is the distance between the surfaces measured from the mean of asperities heights, and the one due to the dielectric layer of thickness s. However, this last contribution is negligible compared to the former one due to the different thickness. The total non contact capacitance, which is the sum of all capacitances in the void regions, is given by:

$$C_{n-c} = \frac{\epsilon_0 A_n (1 - A^*)}{d} \tag{3.13}$$

where $A_n(1-A^*)$ is the total non contact area. The non linear resistor is introduced due to several physical mechanisms like field emission or gas breakdown. If the contact pressure increases a lot, it could happens that in some contact points the oxide film breaks and we have a MM contact. In this case, the equivalent circuit is slightly different from the first one:

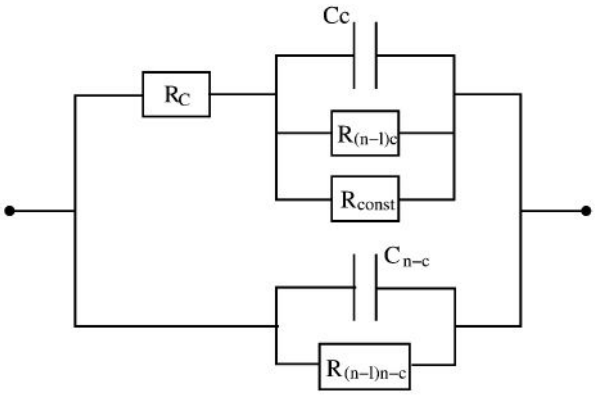

Figure 3.5. Equivalent circuit model of a contact junction when $\alpha-$spots are present

The only difference is the presence of a resistance R_{const} connected in parallel with the capacitor C_c and the non linear resistor $R_{(n-l)c}$. The total resistance due to N_c asperities is given by:

$$R_{const} = \frac{\rho_1 + \rho_2}{4N_a N_c a_{spot}} = \frac{\rho_1 + \rho_2}{4N_c\sqrt{\frac{A_{MM}}{\pi N_c}}} \tag{3.14}$$

where N_a and a_{spot} are, respectively, the number and the average radius of $\alpha-$spots and A_{MM} is the total area of MM contact, which take into account the cracking phenomenon according to the following expression:

$$A_{MM} = A_n A^* \left(\frac{\bar{l}/s}{1+\bar{l}/s}\right)^{\alpha} \tag{3.15}$$

with α the cracking rate of the oxide film in function of the contact pressure and $\bar{l}$ the mean deformation of microasperities given by:

$$\bar{l} = \int_{d^*}^{\infty} (z^* - d^*)\phi^*(z^*)dz^* \tag{3.16}$$

But, about this equivalent circuit model, literature is quite confusing. In fact, several papers have been published about passive intermodulation and each one proposes a different equivalent circuit model. For example, Yang and Wen proposed another equivalent circuit to model a tight contact between two rough surfaces [7]:

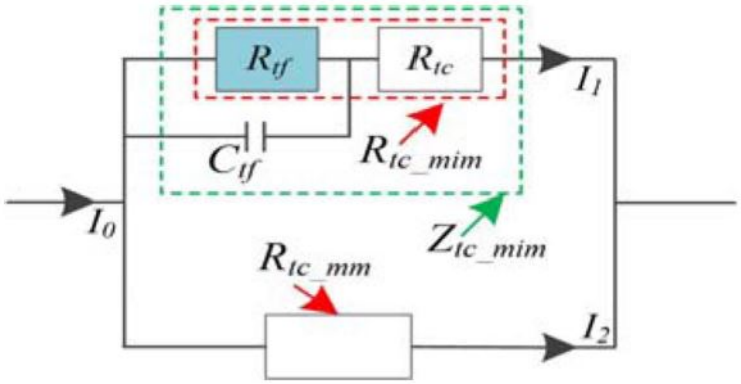

Figure 3.6. Equivalent circuit model in case of tight contact

where the upper branch models MIM contacts while the lower one MM contacts. If instead of considering a tight contact, we consider a loose contact, the equivalent circuit is the one reported in Fig.(3.7).

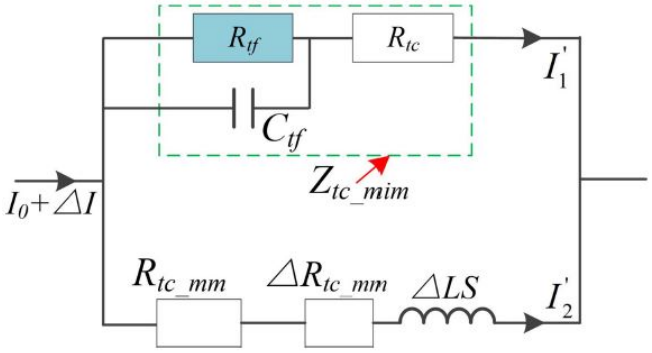

Figure 3.7. Equivalent circuit model in case of loose contact

As we can notice, the most significant change is the presence of an inductance, which is absent in the previous circuits. The presence of an inductance was also considered by Woody during his research project in 1982 at Georgia Institute of Technology. In his studies about intermodulation sources, he presented the circuits reported in Fig.(3.8) to model a MIM contact.

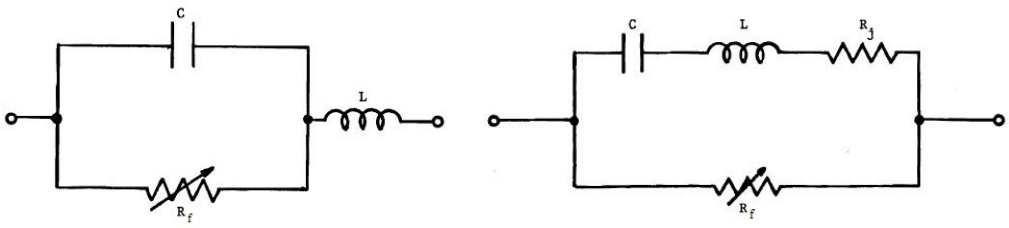

Figure 3.8. Two equivalent circuit models for MIM contact

The most important element, which is common to all shown circuits, is the non linear resistance, which is the effective PIM source. As explained before, the arise of PIM frequencies in the output current spectrum is due to the non linearity of some passive components in the system. Such a non linearity is reproduced by this non linear resistor R_f, whose characteristic is similar to the one reported in Fig.(3.9), [8].

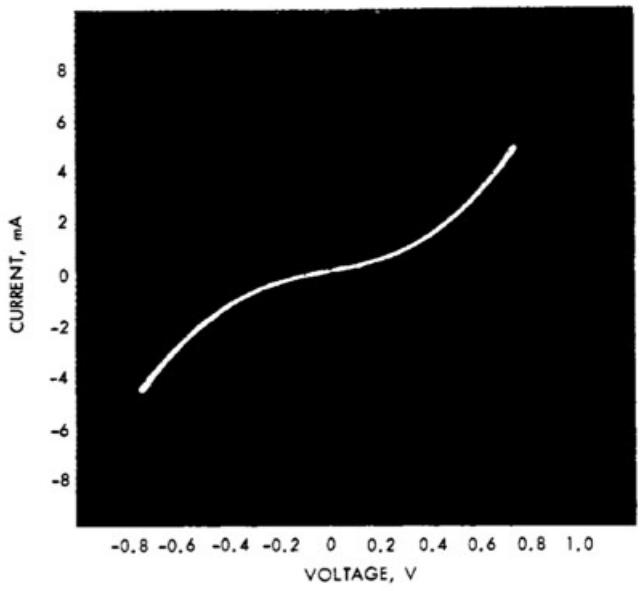

Figure 3.9. Non linear I-V characteristic

This non linear I-V characteristic of conductance $G_f(v) = R_f^{-1}(v)$ is modelled via the following polynomial expansion [1][7][9]:

$$i(t) = \sum_{k=1}^{N} G_{f,k} \cdot v^k(t) \tag{3.17}$$

where coefficients $G_{f,k}$ are estimated via a set of mathematical relationship based on a full-knowledge of the structure under modeling and taking into account the metallization material, the thickness of the oxide layer and the area of contact. From a practical point of view, this non linear resistor is nothing more than a controlled current generator, piloted by the voltage across itself. The presence of so many different circuit models means that there is not a unique consensus in literature and this leads to the issue of how to estimate circuit parameters in a proper way. Furthermore, the main issue is related to the several effects which have been identified as sources of PIM frequencies and to the difficulty in isolating experimentally these mechanisms.

3.1 Tunnel Effect

Among the cited effects which could be responsible for the arise of PIM, the tunnel current through the oxide film could be one of the most critical and studied in literature. In fact, in several papers this phenomenon is indicated as the main cause of PIM generation, especially if the layer is very thin (about few nanometers). The presence of the dielectric layer introduces a potential barrier between the surfaces which prevents the flow of electrons, as depicted in Fig.(3.10):

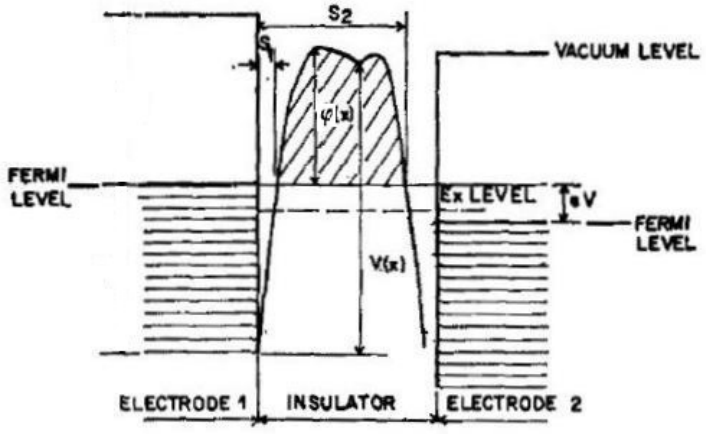

Figure 3.10. General potential barrier due to the presence of a dielectric film

where $\varphi(x)$ is the height and $\Delta s = s_2 - s_1$ the effective thickness of the barrier. But, if the oxide film is thin enough, electrons can flow through this barrier, giving rise to the socalled tunnel current. Tunneling current was studied in depth by Simmons in the early 1960s [6], who provided a formula for the tunnel current density. For sake of simplicity, we supposed to deal with a rectangular potential barrier, like the one reported in Fig.(3.11).

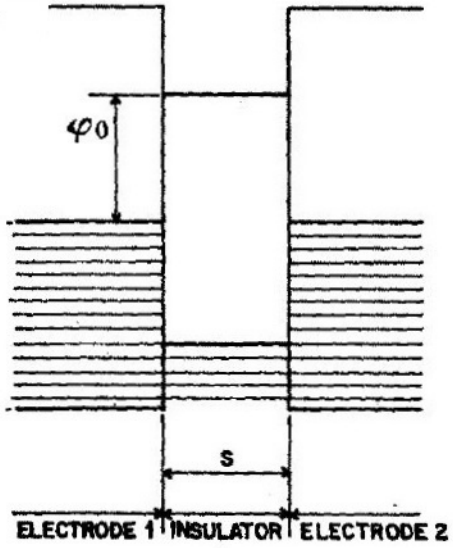

Figure 3.11. Rectangular potential barrier

In the figure, s is the thickness of the insulating layer and φ_0 the height of rectangular barrier. If V is the voltage across the oxide layer, we can distinguish two cases:

- $0 < V < \varphi_0$
- $V > \varphi_0$

In the first case, the tunnel current density is given by:

$$\begin{aligned} J = & \left(\frac{6.2 \times 10^{10}}{s^2}\right)\{(\varphi_0 - V/2)exp[-1.025s(\varphi_0 - V/2)^{1/2}] + \\ & - (\varphi_0 + V/2)exp[-1.025s(\varphi_0 + V/2)^{1/2}]\} \end{aligned} \tag{3.18}$$

While, in the second case is given by:

$$J = 3.38 \times 10^{10} \left(\frac{F^2}{\varphi_0}\right) \left\{ exp\left(-0.689 \frac{\varphi_0^{\frac{3}{2}}}{F}\right) + - \left(1 + \frac{2V}{\varphi_0}\right) exp\left[-0.689 \frac{\varphi_0^{\frac{3}{2}}}{F} \left(1 + \frac{2V}{\varphi_0}\right)^{\frac{1}{2}}\right] \right\} \tag{3.19}$$

where $F = V/s$ is the field strength in the insulator. J is expressed in A/cm^2, φ_0 in eV and s in Å units. In order to obtain the current, it's sufficient to multiply the density J by the contact area A. Thanks to the theory of tunneling effect, we were able to explain the results shown in [1] and reported in Fig.(3.12).

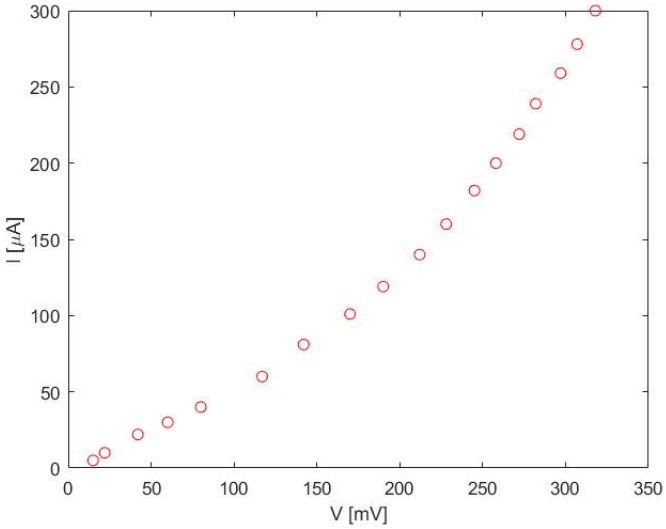

Figure 3.12. Experimental data

Thanks to a Matlab script in which are implemented the previous equations (3.18) (3.19) for the tunnel current, it appears that the tunnel effect could explain the behaviour:

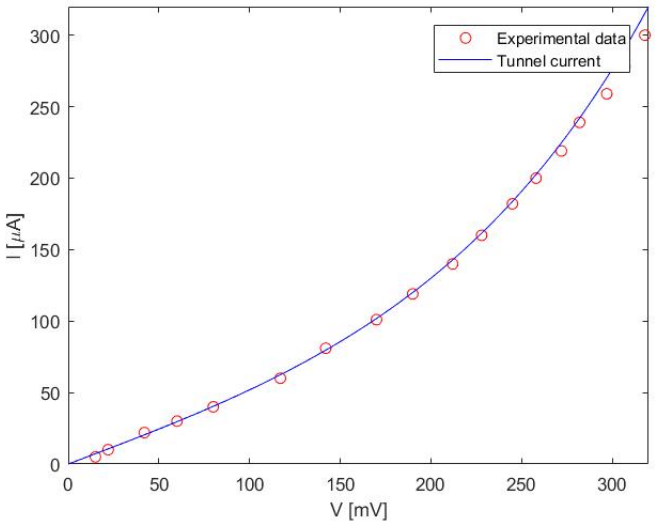

Figure 3.13. Tunnel current curve and experimental data

This curve was obtained setting the parameters as follows:

Parameter	*Value*
φ_0 [eV]	0.86
s [Å]	25.6
A [cm^2]	0.0168

Even if we were able to reproduce results in [1], the problem is that several parameters need to be accurately estimated and controlled (especially the thickness of the oxide film because tunnel current change a lot with a small variation of the latter) to get an accurate model of the tunneling effect thanks to the equations (3.18) and (3.19). In fact, Bond and Guenzer for their experimental measurements, used a well controlled fabrication scenario that allowed them to estimate in a precise and reliable manner all required parameters. But such a scenario, with a pure oxygen chamber used for oxidation and vacuum evaporation for fabrication of aluminium layers, it's really hard to reproduce and it does not represent a realistic scenario. The problem is that the tunnel effect, although indicated in several papers as the main source of PIM products, is not able to fully explain experimental data. Guenzer [10] strongly criticized Higa's results [8], because based on equations which "have been inconsistently expanded". Indeed, as explained before, tunnel effect is not the only

PIM source. The non linear behaviour could be explained as the combination of the several microscopic effects cited above (tunnel effect, electro-thermal effects, etc...). In addition to these, also another effect has to be mentioned because contributes to determine this non linear behaviour: is the non linear conductivity. In PCB traces, this is due to the presence of copper foil structure, surface roughness, foil-dielectric interfaces and finishing of the etched traces [11]. So, in addition to the problem of accurately estimating all parameters, there is the problem of isolating experimentally all these effects which contribute to the generation of PIM. Under these conditions, it becomes impossible to develop a reliable model able to fully explain the non linear behaviour of such a system. Since a physical-based model involves so many efforts due to the issues cited above, we can try to develop a model thanks to a behavioural characterization.

Chapter 4

Behavioural-based model

The key point of this chapter is to develop an equivalent circuit model of a metal-metal contact starting from experimental data obtained from several experiments performed in laboratory. Furthermore, these results were validated via simulations using the software *CST Microwave Studio*.

4.1 Measurements setup

The setup used to perform the following measurements is shown in Fig.(4.1):

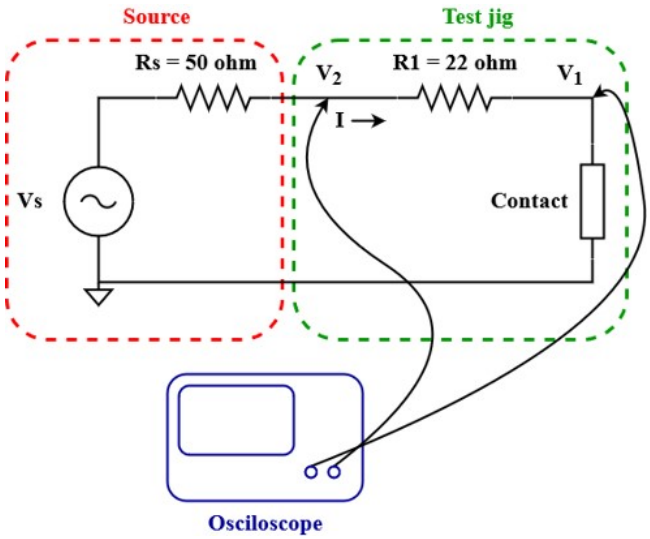

Figure 4.1. Measurement setup scheme

where the test jig is highlighted with the green square, while the red one corresponds to the source. The first step was to check the non linear behaviour of the model and find the relative I-V characteristic. In order to do this, a DC characterization of the model was performed. Indeed, the main assumption made in all the studied papers is that the non linear I-V characteristic of the contact is constant in frequency and therefore it can be estimated in DC. As source was used a signal generator with an internal resistance R_s equal to 50Ω. The input signal was a triangular voltage waveform with amplitude $10V_{pp}$ at low frequency (50Hz). The test jig consists of the contact in series with a resistor R_1 of 22Ω. This latter is needed in order to make possible the measurement of the current that flows through the contact. Measurements were carried out using an oscilloscope with channel 2 connected directly to source output V_2 and channel 1, thanks to a probe, to detect the contact voltage V_1. Setting the oscilloscope in the XY mode, it is possible to see immediately if the I-V characteristic is linear or not. The monitor of the oscilloscope does not show directly the I-V characteristic, because in the two channels there are two voltages. In order to obtain the current, we have to use the following formula:

$$I = \frac{V_2 - V_1}{R_1} \tag{4.1}$$

But, since the current is directly proportional to the measured voltage, if the characteristic shown on the oscilloscope's monitor is linear, also the I-V characteristic will be linear. This is useful in order to understand immediately if the test jig has a non linear behaviour. A picture of the described setup is reported in Fig.(4.2).

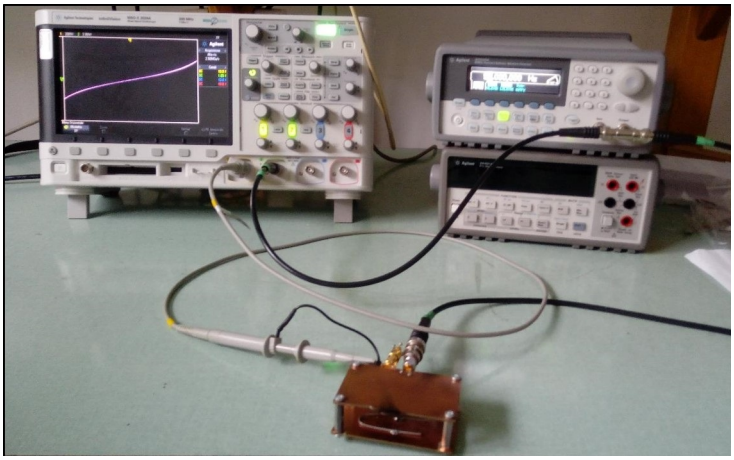

Figure 4.2. Measurement setup

This is the setup in common with all experimental tests we performed.

4.2 Test 1: copper strips

The first test we performed was characterized by a very simple setup: 2 strips of oxidized copper in contact. We decided to use the copper instead of other materials more diffused in literature, like aluminium, for sake of simplicity. Indeed, it is easier to oxidize the copper instead of aluminium. The pieces of copper used for the test had the following dimensions:

Parameter	**Value**
Length	6 cm
Width	1 cm
Thickness	0.2 mm

These pieces of copper were oxidized in different ways in order to change also the thickness of the grown oxide film. They were oxidized in the following four ways:

- They have been left in a room for 48 hours;
- They have been left outside for 48 hours;
- They have been put in the oven for about 20 minutes at temperature of 200 °C;
- They have been put in the oven for about 20 minutes at temperature of 200 °C and then put in cold water.

The setup is reported in Fig.(4.3).

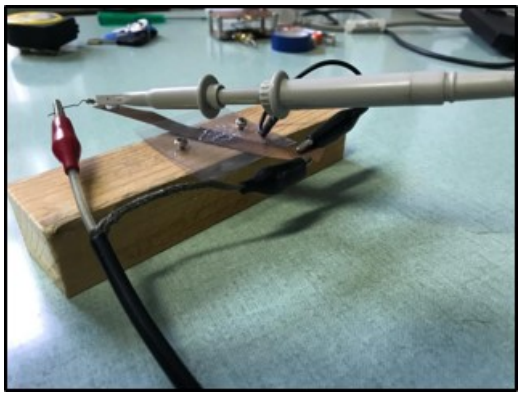

Figure 4.3. Test 1: Two copper strips in contact

A 22Ω resistor was soldered with a piece of copper and this latter put in contact with another strip of oxidized copper thanks to a piece of wood that works as support. The input triangular signal was connected to the resistor and the probe between the resistor and the piece of copper in order to measure the voltage across the contact. Setting the oscilloscope in the XY mode, we can see the characteristic, which shows a linear behaviour as we can see in Fig.(4.4):

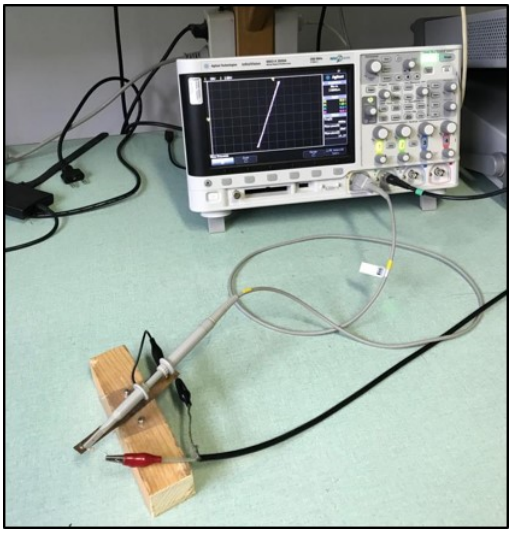

Figure 4.4. Test 1: Linear characteristic of two copper strips in contact

In this case there is not the presence of PIM as we can notice from the linear behaviour of the system. This test was replicated for each piece of copper oxidized in the different explained ways, showing always a linear behaviour.

4.3 Test 2: steel wires

For the second test, we decided to replicate a setup present in [12], where two metal wires are connected as shown in Fig.(4.5):

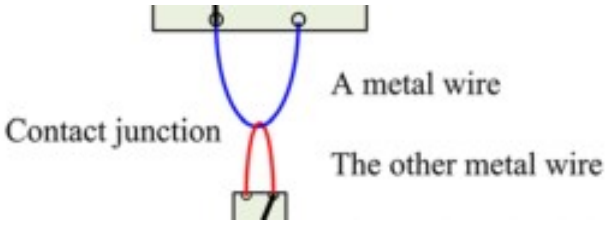

Figure 4.5. Test 2: Layout of the experiment setup

In this case, in the place of the copper, were used two wires of steel with diameter $d = 0.7$mm put in contact as shown in Fig.(4.6):

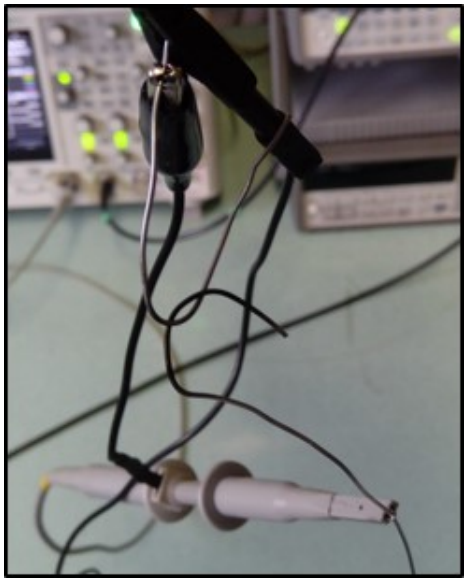

Figure 4.6. Test 2: Two metal wires in contact

In this case the contact area between the two wires was pre-oxidized by means of a flame, in order to grow the wanted oxide film. The 22Ω resistor was connected to one of the wire. Unlike the first test, in this case the system shows a slightly non linear characteristic:

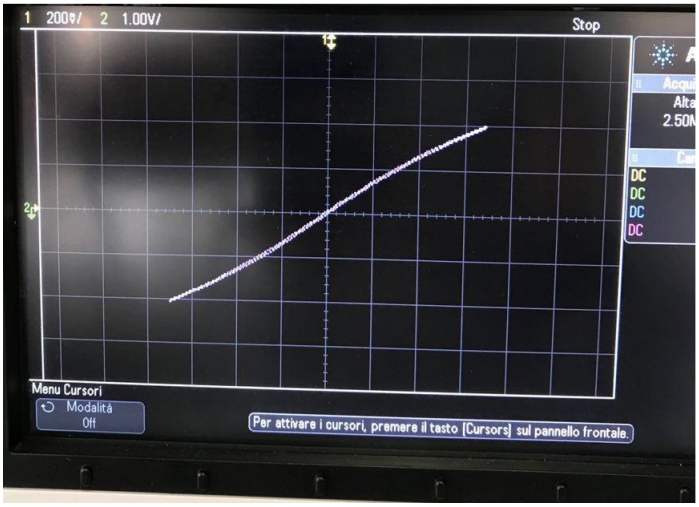

Figure 4.7. Test 2: Non linear characteristic behaviour

We were able with this setup to show the non linear behaviour of such a contact even if, at first analysis, we would have expected that the non linearity was in the opposite side, as explained in the tunnel effect theory. In reality, this kind of situation was already described by Higa [8], who observed in MIM junctions two kinds of non linearities as reported in Fig.(4.8):

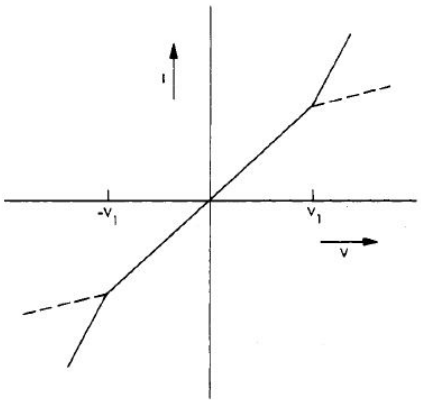

Figure 4.8. Two kinds of non linearities which are generated by MIM junctions

As we can notice from Fig.(4.7) and Fig.(4.8), for small voltages the current is a linear function of voltage, while for values of voltage exceeding a minimum value, indicated in Fig.(4.8) as V_1, the conductance becomes non linear, leading to an

higher (solid line) or lower (dashed line) value. The non linear properties for both cases are only slightly different. The main issue related to this test was the setup itself. Indeed it looks very unreliable due to the fact that it is very unstable and it is not possible to have accurate results.

4.4 Test 3: steel copper contact

In order to have a more reliable jig, the two wires were substituted by a new setup, in which a steel wire was placed between two copper PCBs. By doing so, we modified not only the setup, but also the kind of contact. Indeed, we replaced the old steel-steel contact with a steel-copper one, as depicted in Fig.(4.9):

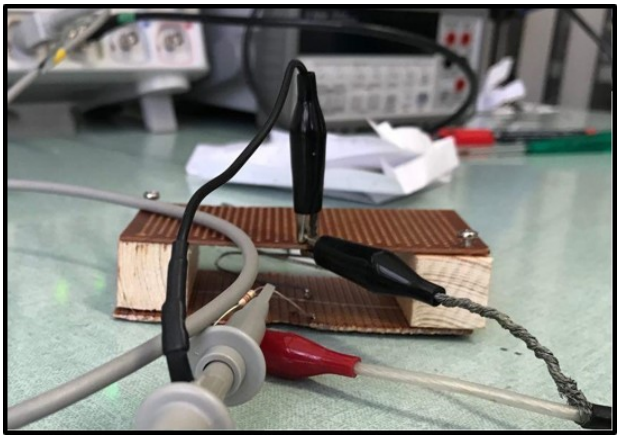

Figure 4.9. Test 3: Steel wire in contact with a copper PCB

The setup was built using two equal pieces of copper PCB, with size 7.5cm×5cm placed at a distance of about 2cm thanks to two pieces of wood as a support. To make the setup more stable, these copper PCBs where fixed on wood by using two screws on the opposite corners. On the inner side of one of the copper pieces were soldered the usual 22Ω resistor and one extremity of a steel spring-clip with diameter $d = 1$mm. The other one is used to perform the wanted contact steel-copper. As we did for *Test 2*, also in this case the contact area was treated by a flame in order to grow an oxide film. Exciting the system with the triangular waveform described before, what we observed in the oscilloscope's monitor is reported in Fig.(4.10):

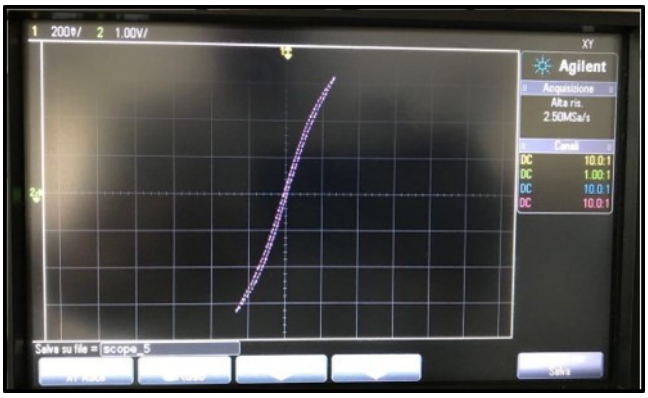

Figure 4.10. Test 3: Non linear characteristic behaviour

In this case the non linearity of the curve is more evident. The main advantage of this setup with respect to the previous one is the reliability. Indeed, this last model is more reliable and reproducible. Instead, the main issue is related to the absence of a common ground.

4.5 Test 4: 2^{nd} version steel copper contact

An update of the previous version setup was needed to solve the problem of the absence of common ground and to make the whole system even more reliable. In this new model the pieces of wood were replaced with 4 cylinders of steel in the corners fixed by using screws. In this case, having steel instead of wood, it was necessary to isolate the corners, in order to not have connections between the ground planes and the copper. This was realized thanks to several cuts in the copper near the corners. In this way, the four cylinders act not only as support between the two PCBs, which have the same size of the ones used in the previous test, but also as connection between the two ground plane. Even if we replaced the support, the distance between the copper PCBs has remained unchanged. This new setup is reported in Fig.(4.11):

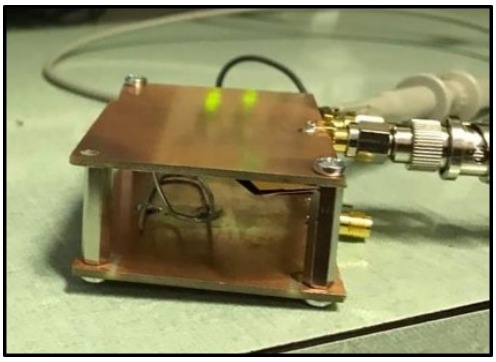

Figure 4.11. Test 4: Steel wire in contact with a copper PCB

The main difference is the presence of three ports SMA: two soldered on the upper part, the last one in the lower part. The ports on the top were used one for the application of the input signal from the function generator and the other one for the connection of the 22Ω resistor. This latter in particular was soldered between a cut in the copper in order to replicate the same setup scheme of the previous tests. The last port on the bottom part was soldered for the completeness of the model. Indeed, in this way, it is possible to put a load after the steel-copper contact, but this situation is outside the scope of our analysis. With this new model we obtained the characteristic reported in Fig.(4.12):

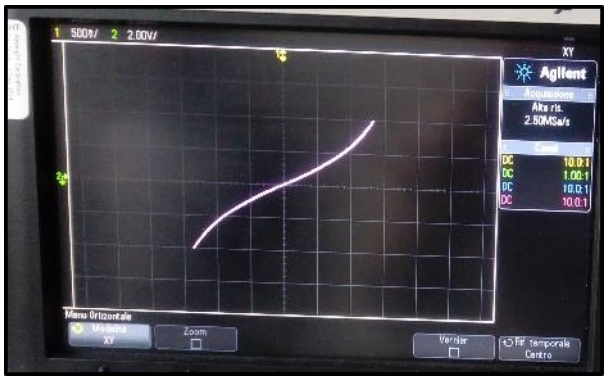

Figure 4.12. Test 4: Non linear characteristic behaviour

As we can notice, in this case the system shows a non linearity which is in the opposite side with respect to the previous tests. Among the explained setup, this

latter is for sure the most stable and reliable. It is for this reason that we decided to focus our attention on it.

4.6 Derivation of an equivalent circuit for the contact

As explained, the key point of this analysis is to find a model that could fully describe a contact between two metal surfaces. Such a model should be able to take into account:

- Dynamic effect
- Non linear effects

The first effect mainly affect the behaviour of the system at high frequency, while the second one is more important at low frequency or within the DC behaviour. As difficult as it is, we are looking for a general and rigorous modeling scheme able to assess all circuit parameters starting from experimental data. We started our analysis considering the simplest possible circuit model and depicted in Fig.(4.13):

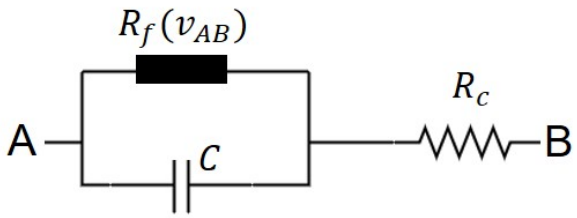

Figure 4.13. Simplest circuital model

It consists of a capacitor C, a resistor R and a non linear resistor $R_f(v_{AB})$, which is function of the voltage applied across the two terminals A e B. The resistor is put in series with the parallel branch composed by the capacitor and the non linear resistor. The first step was a characterization of the model explained in *Test 4* in the DC domain. Therefore, the characteristic of the non linear resistor was estimated via a set of DC excitations. In this case the capacitor is an open circuit:

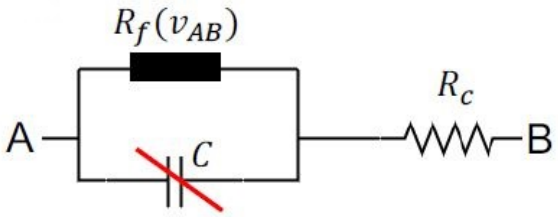

Figure 4.14. Circuital model with an open circuit instead of capacitor

To do this a signal with a very low frequency was used (50Hz). Under these conditions, the capacitor can be seen as an open circuit. The obtained curve was exported and, with a Matlab script which implements equation (4.1), we were able to estimate the current and plot the resulting I-V characteristic, which is reported in Fig.(4.15):

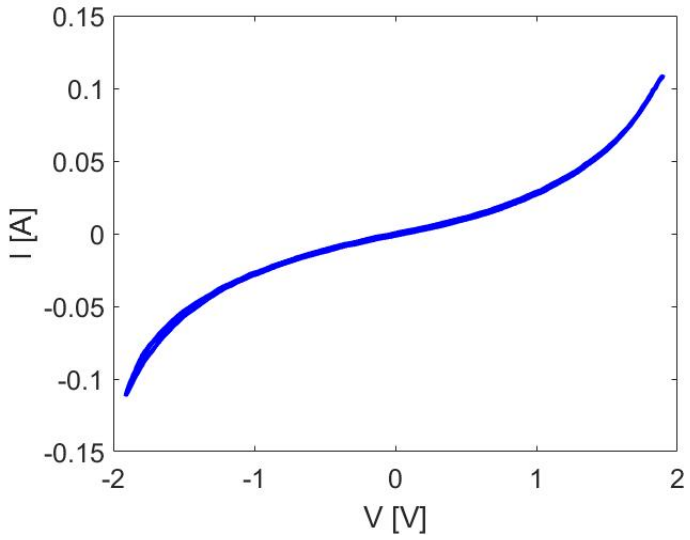

Figure 4.15. Measured I-V characteristic of *Test 4*

In order to fully characterize the non linear resistor behaviour, thanks to a Matlab script in which the function *"polyfit"* is used, we performed a polynomial fitting of the measured curve:

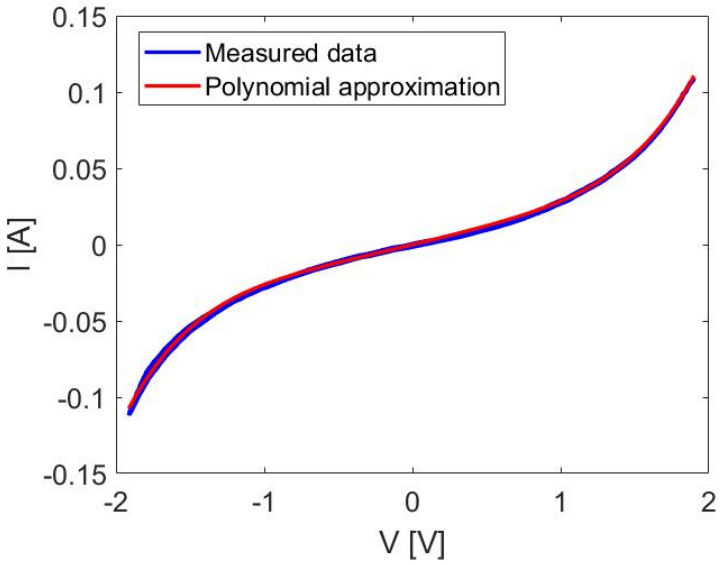

Figure 4.16. Comparison between the measured characteristic (blue curve) and the polynomial approximation (red one)

This fitting was performed using a 5^{th} order polynomial by neglecting the bias term:

$$i(v_{ab}) = 0.0020v_{ab}^5 - 0.0001v_{ab}^4 + 0.0019v_{ab}^3 + 0.0013v_{ab}^2 + 0.0234v_{ab} \tag{4.2}$$

As we can notice, coefficients of the even terms are very close to zero. Indeed, the I-V characteristic of a realistic contact must be an odd function. Once plotted the I-V characteristic, in order to fully characterize the model, we have to compute the S-parameters, which are needed to estimate the dynamic behaviour of the system. The main issue related to this step is due to the non linearity behaviour of the model. In fact, the S-parameters are defined only for linear devices. So, we have to ensure that we are working around the linear region of the characteristic, that is highlighted in Fig.(4.17) by the green square.

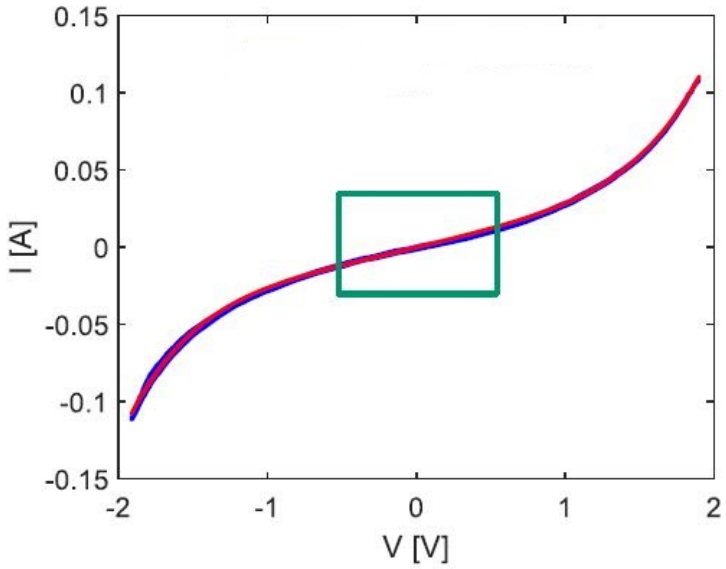

Figure 4.17. Linear region of the I-V characteristic (green square)

Looking at Fig.(4.17), the linear behaviour is guaranteed only if we deal with small voltages, within the range defined by:

$$-300\text{mV} < V < 300\text{mV}$$

In order to compute these parameters, we used a vector network analyzer (VNA) connected to the test jig through the input port, as shown in Fig.(4.18).

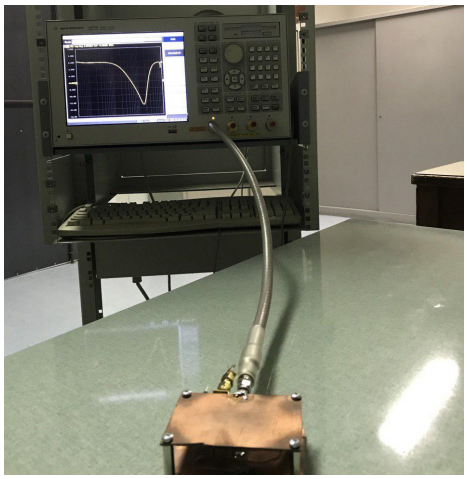

Figure 4.18. One port characterization of the model by using VNA

Thanks to the VNA, we were able to fully characterize the device, measuring the S-parameters in magnitude and phase. In this way we could analyze the transmission and the reflection of signals. It is important, before proceeding with the measurements, to set the correct range of frequency in which we want to characterize the jig. As frequency range we set from 300kHz to 1GHz. In this way we obtained a characterization of the system through the variation of the input impedance Z_{in} given by:

$$Z_{in} = Z_0 \frac{1 + S_{11}}{1 - S_{11}} \tag{4.3}$$

where Z_0 is equal to 50Ω. The obtained curves of magnitude and phase of the input impedance Z_{in}, expressed in degree, in function of the frequency are reported, respectively, in Fig.(4.19) and Fig.(4.20).

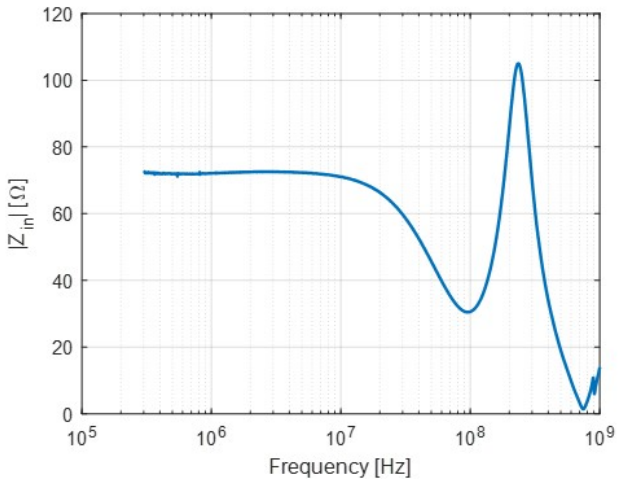

Figure 4.19. Magnitude of the input impedance ($|Z_{in}|$)

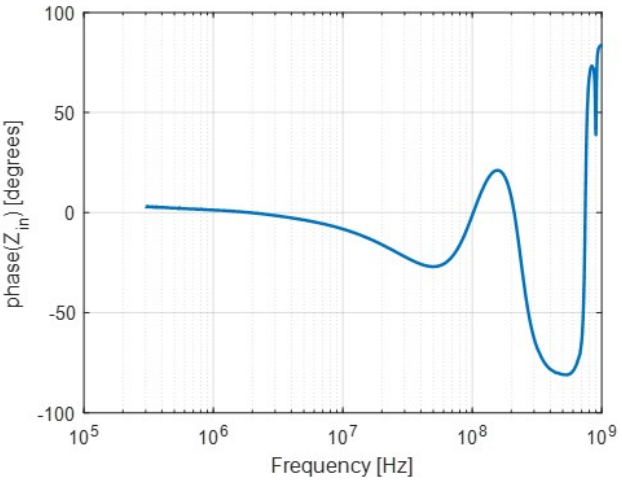

Figure 4.20. Phase of the input impedance ($\angle Z_{in}$)

The main issue is due to the fact that, by doing so, we measured the input impedance of the whole test jig. But, we are interested in characterizing the contact, not the whole system. However, we can overcome this issue analyzing the voltage v_1 across the contact and the current i through this latter, depicted in the scheme of Fig.(4.21).

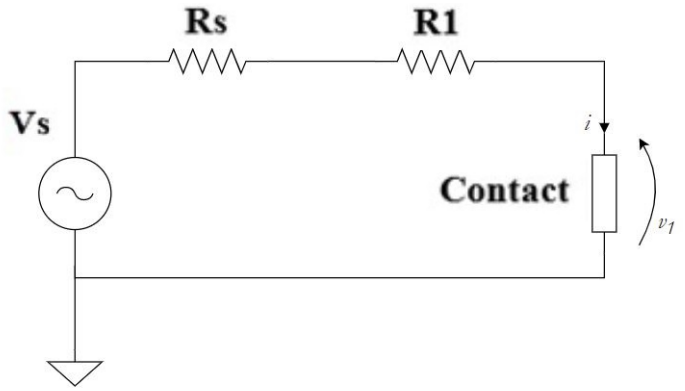

Figure 4.21. Circuit scheme with the current i through the contact and the voltage v_1 across the contact

Indeed, for a generic periodic excitation with fundamental frequency $\omega = \omega_0$, we can write its Fourier series expansion. In this way, the voltage v_1 and the current i can be written respectively as:

$$v_1(t) = \sum_{n=-N}^{N} V_{1,n} e^{jn\omega_0 t} \tag{4.4}$$

$$i(t) = \sum_{n=-N}^{N} I_n e^{jn\omega_0 t} \tag{4.5}$$

By doing so for the waveforms of current through the contact and voltage across the contact acquired with the oscilloscope, varying the angular frequency $\omega_0 = 2\pi f_0$ of the excitation signal, we were able to define the "fundamental impedance" thanks to this set of measured waveforms. In our case, eleven frequencies f_0 were considered: 50Hz, 500Hz, 1kHz, 5kHz, 10kHz, 50kHz, 100kHz, 500kHz, 1MHz, 10MHz and 80MHz. From each measured value, we obtained the respective impedance of the contact Z_x for the corresponding value of angular frequency as the ratio between the fundamental components of the Fourier representation of voltage time-domain waveform and the one of the current, as expressed by the following equation:

$$Z_x(\omega) = \frac{V_{1,1}}{I_1} \tag{4.6}$$

By repeating this procedure for every measured value of voltage and current at each angular frequency considered, we were able to plot the contact impedance Z_x in magnitude and phase:

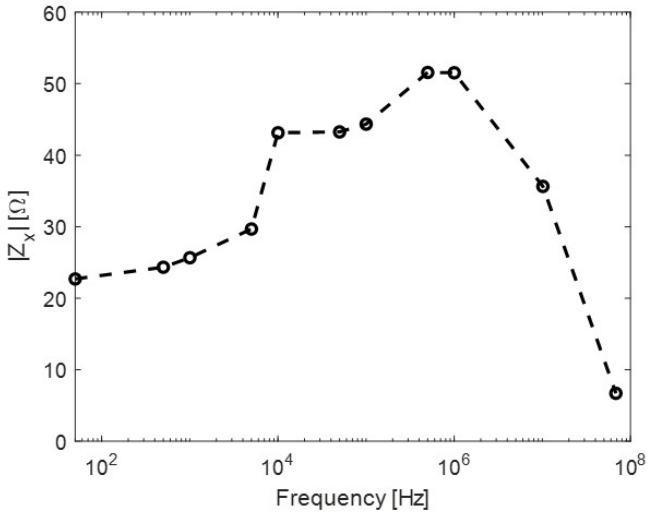

Figure 4.22. Magnitude of the contact impedance ($|Z_x|$)

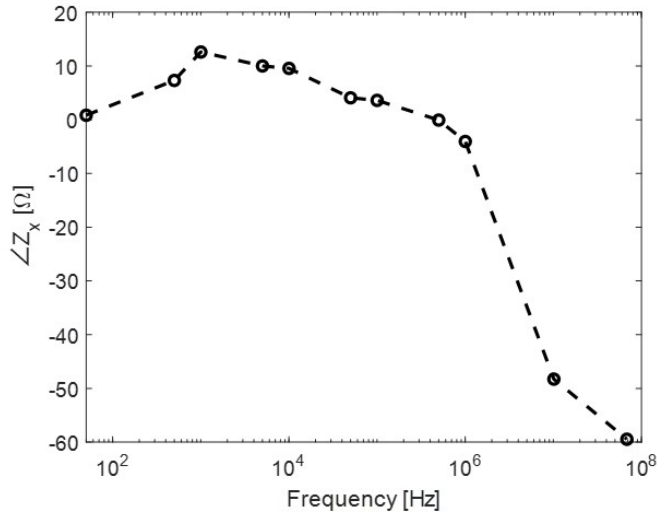

Figure 4.23. Phase of the contact impedance ($\angle Z_x$)

Since the used angular frequencies belong to a very wide range, for the plots of Fig.(4.22) and Fig.(4.23), a semilogarithmic scale for the x-axis was used. Looking at the previous plots, specifically the plot of the phase, and focusing on the variation of this latter, we can clearly distinguish two regions:

- The first region, from 50Hz to about 500kHz, in which the phase is positive and, so, it shows an inductive behaviour
- The second one, from 500kHz to 80MHz, that is instead negative and, so, it describes a capacitive behaviour

These two different behaviours are highlighted in Fig.(4.24), respectively by a green shape and a red one:

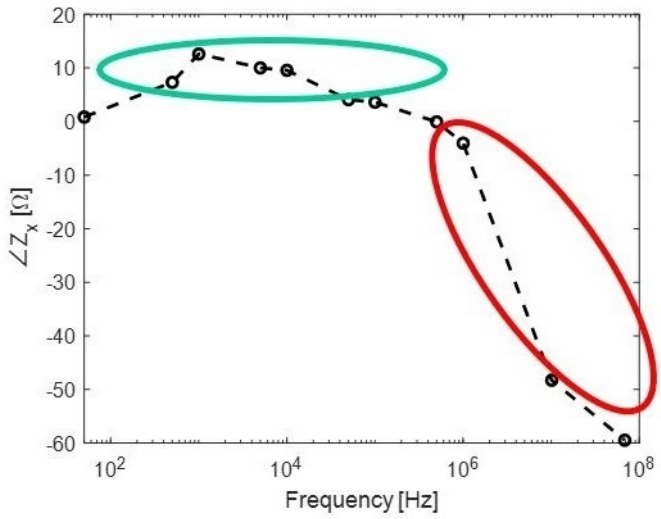

Figure 4.24. Inductive behaviour region (green shape) and capacitive behaviour one (red shape)

It is clear that the previously considered equivalent circuit, reported in figure (4.13) is not able to provide the same impedance behaviour and the proposed circuit must be improved. Indeed, this latter does not allow to predict the voltage waveform across the non-ideal contact and the current waveform through the same. The previous circuit was improved introducing, in series with the old one, a parallel RLC circuit. The resulting equivalent circuit is depicted in Fig.(4.25):

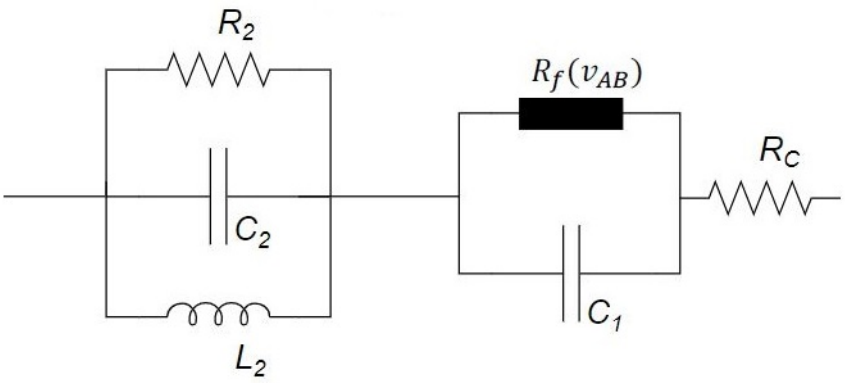

Figure 4.25. New equivalent circuit model

Indeed, this new circuit is able to approximate the variations of the measured contact impedance $Z_x(\omega)$. The values of circuit's parameters have been obtained thanks to several simulations, in order to choose the ones that best approximate the trend of the contact impedance:

Parameter	**Value**
R_C	1Ω
C_1	100pF
R_2	27Ω
C_2	500pF
L_2	700μH

In order to simulate it with the tool Spice, the non linear resistor $R_f(v_{AB})$ was replaced with a voltage-controlled current generator, as shown in Fig.(4.26).

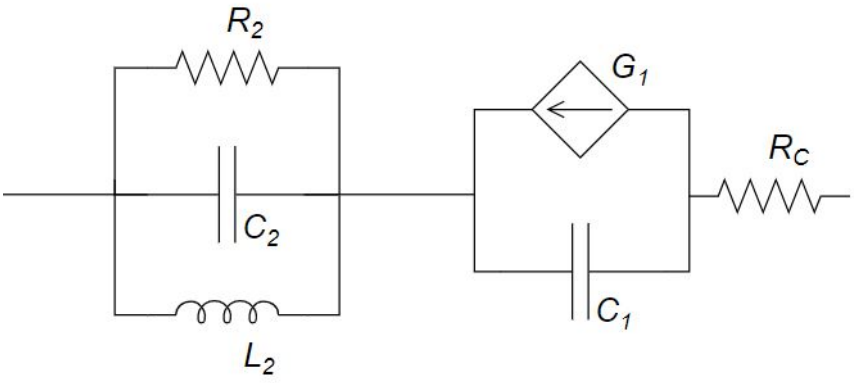

Figure 4.26. Equivalent circuit model with voltage-controlled current source

The current generator G_1 is driven by the voltage across itself through the equation (3.17), in which the coefficients $G_{f,k}$ are the ones reported in (4.2), estimated from the measured I-V characteristic in DC. The magnitude and the phase of the contact impedance Z_x obtained from the simulation of the equivalent circuit are compared with the measured ones:

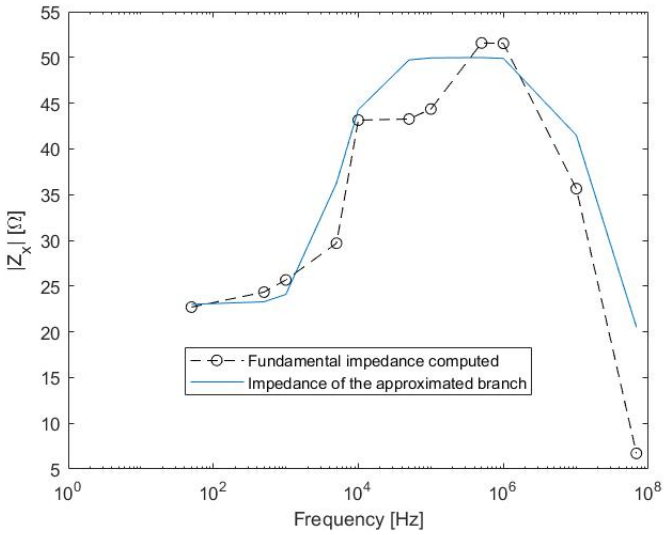

Figure 4.27. Comparison between the magnitude of the contact impedance ($|Z_x|$) obtained from simulation (blue line) and the measured one (dashed line)

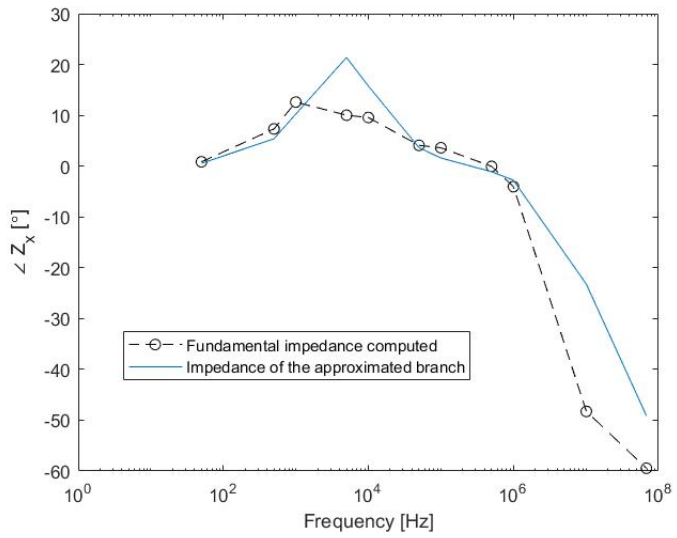

Figure 4.28. Comparison between the phase of the contact impedance ($\angle Z_x$) obtained from simulation (blue line) and the measured one (dashed line)

Once characterized the contact from the electrical point of view, the last step was try to observe and measure PIM products in the output spectrum. In order to do this, we used a spectrum analyzer, a device able to show the spectrum of a signal. It is able to measure the magnitude of an input signal (on the y-axis) in function of the wanted frequency range setted (on the x-axis). To do this, we used again the signal generator connected to the jig through the same port as before. As input, we used a sinewave signal with amplitude of 10V_{pp} and frequency $f = 1\text{MHz}$. The spectrum analyzer was connected to the jig thanks to a probe. The frequency range was setted from 0 to 10MHz and the resolution bandwidth (RBW) equal to 3kHz. The resolution bandwidth in a spectrum analyzer is the frequency span of the final filter which is applied to the input signal. We decided for such a small value in order to provide finer frequency resolution and improve the capability to differentiate signals that have frequencies which are closer together. The resulting spectrum of the voltage on the contact is reported in Fig.(4.29).

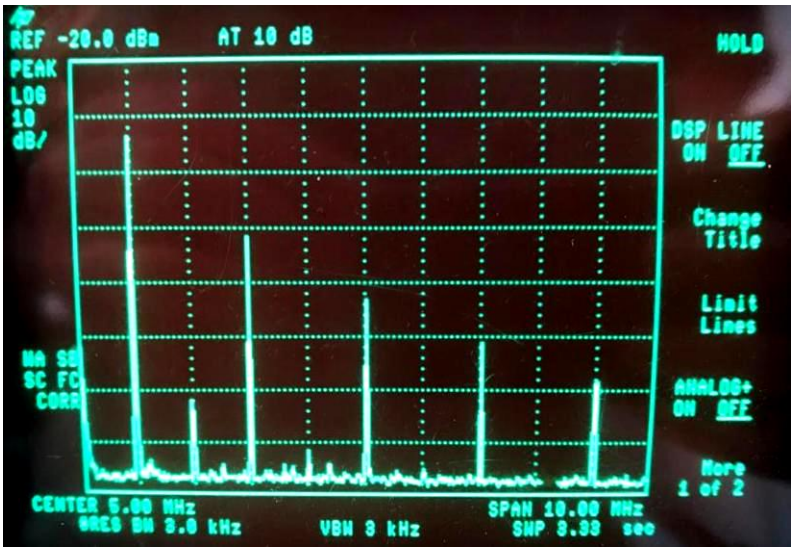

Figure 4.29. Spectrum of the voltage on the contact

As we can clearly notice in Fig.(4.29), the output spectrum does not present only the fundamental frequency component $f = 1\text{MHz}$, but, as we expected, there are other frequency components at:

- $f_1 = 3 \times f = 3\text{MHz}$
- $f_2 = 5 \times f = 5\text{MHz}$
- $f_3 = 7 \times f = 7\text{MHz}$
- $f_4 = 9 \times f = 9\text{MHz}$

Once checked the presence of distortion in the output spectrum in the case of a single input signal, we were interested in investigate this latter when, instead of a single input signal, we have two different signals with close frequencies. This was possible thanks to another function generator and a T-connector, in order to excite the jig with two sinusoidal waveforms. The two signal generators were setted with two sinewaves of amplitude 10V_{pp} and frequencies $f_1 = 1\text{MHz}$ and $f_2 = 1.5\text{MHz}$. The frequency range and the resolution bandwidth have remained unchanged. The resulting contact voltage spectrum is reported in Fig.(4.30).

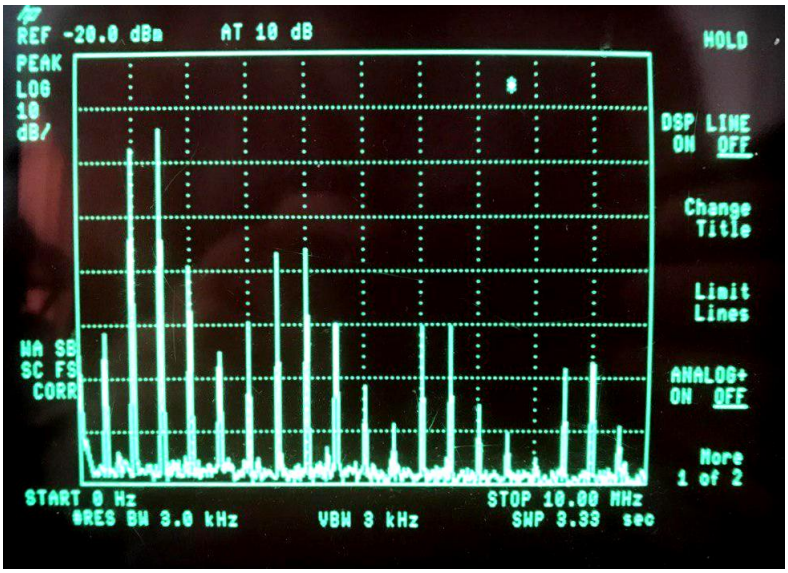

Figure 4.30. Spectrum of the voltage on the contact obtained from measurements with two input signals

We can note in the spectrum, the arise of intermodulation frequency components, in addition to the two fundamental ones, given by:

- $2f_1 - f_2 = 0.5\text{MHz}$
- $2f_2 - f_1 = 2\text{MHz}$
- $3f_2 - 2f_1 = 2.5\text{MHz}$

After having developed an equivalent circuit model for the above contact and having noticed the presence of PIM frequencies in the output spectrum of the built jig, the next step was to validate the obtained circuital scheme through simulations, comparing the resulting voltage and current waveforms with the measured ones.

Chapter 5

Validation of the model

Once characterized the contact from the electrical point of view and developed an equivalent circuit model that is able to describe the behaviour of the contact, the next step was to validate this latter through simulations. The software used to perform these simulations is *CST Microwave Studio*, which is a fully featured software package for electromagnetic analysis and design in the high frequency range. Once the model has been realized, a fully automatic meshing procedure is applied before starting the simulation task. Before proceeding with the realization and simulation of the chosen setup, we performed a preliminary test in order to check the feasibility.

5.1 Preliminary simulation

In order to show the presence of PIM products in the output spectrum, the model reported in Fig.(5.1) was simulated in *CST Microwave Studio*.

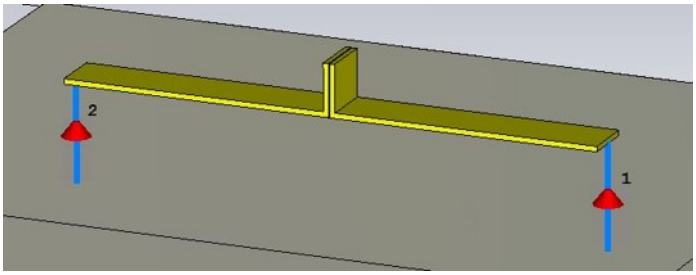

Figure 5.1. Model for the feasibility test in *CST Microwave Studio*

In the above model, two pieces of aluminium (in yellow) are separated by a dielectric

layer of aluminium oxide (Al_2O_3). Two discrete ports (indicated in the figure with two red cones) were put at the extremities of each piece of aluminium, in order to connect them with a ground plane (grey region in the figure), made of a material called *PEC (Perfect Electric Conductor)*. Once setted to *"Open"* the boundary conditions, the *3D* model was simulated using the *"Transient solver"* mode in a frequency range from 0.1MHz to 150MHz and the S-parameters were calculated. Leaving the *3D* mode and going to the *Schematic* one, it was possible, putting a proper port, excite the system with a sinewave signal with amplitude of 10V and a frequency equal to 20MHz. The spectrum of the excitation voltage and the current through the contact are reported, respectively, in Fig.(5.2) and Fig.(5.3).

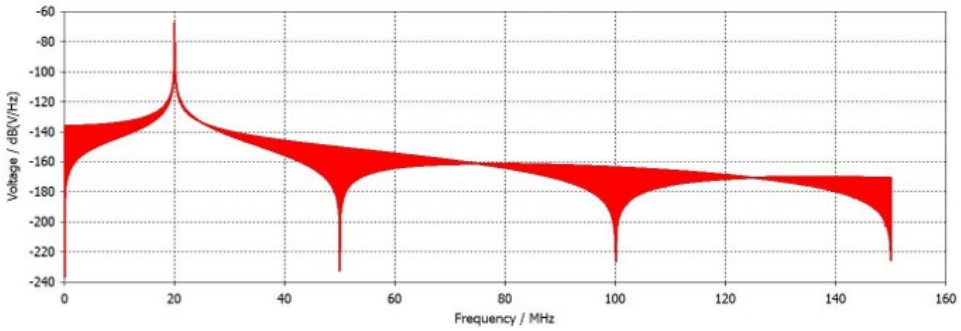

Figure 5.2. Spectrum of the excitation voltage used for the simulation of the setup in figure (5.1)

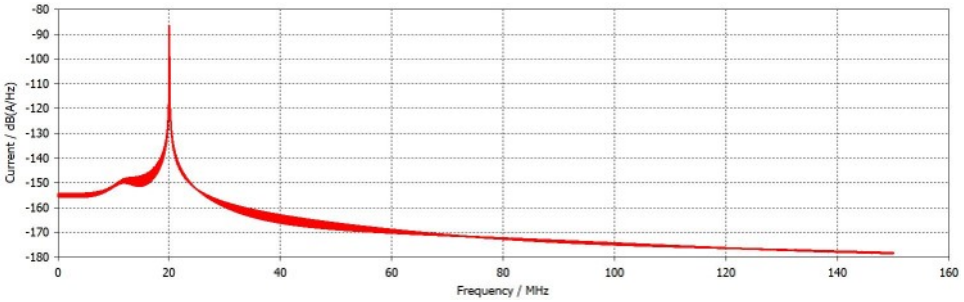

Figure 5.3. Spectrum of the current through the contact of the setup in figure (5.1)

As we can notice from the spectrum of the current and voltage, there is only the fundamental frequency component at 20MHz. Since there is no distortion in the output spectrum, despite what we thought, the system presents a linear behaviour. This lack is due to the fact that *CST Microwave Studio*, like the majority of classical

tools for the full-wave electromagnetic simulation of *3D* structures, is not able to account for the effects which are the sources of PIM products mainly for two reasons:

- Metal-metal contact interface is very thin and hard to mesh
- The microscopic effects, which are responsible for the non linear behaviour of the contact region, are not considered by these full-wave solvers [7]

In order to model the PIM, the only solution is to include a non linear element in the schematic circuit of the simulation. Thus, to do this, only one side of the contact was modelled, as depicted in Fig.(5.4).

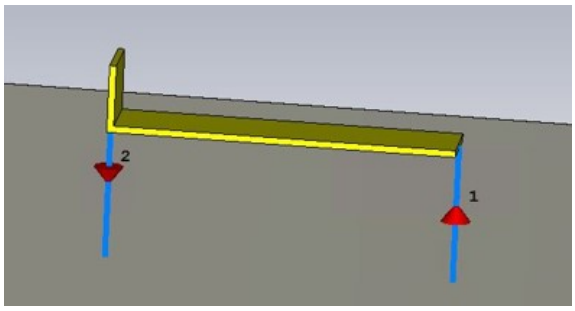

Figure 5.4. Half part of the simulation model

In this case, we implemented only one piece of aluminium, without considering the oxide layer. As we did before, we characterized it in the *3D* space through the *"Transient solver"* mode in the same frequency range of the previous model and with the same boundary conditions. The most significant change is in the *Schematic* representation. Indeed, in this case, instead of having a simple connection between the source port and the built model, there is a non liner *SPICE* block connected with the circuit as depicted in Fig.(5.5).

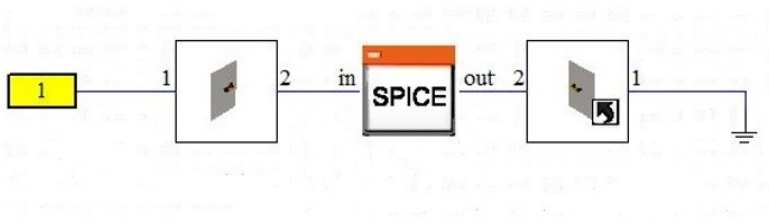

Figure 5.5. Schematic circuit with the non linear *SPICE* block

This *SPICE* block is a voltage-controlled current generator which acts as non linear resistance and was placed between the two aluminium pieces of the model that are in contact. The system was excited by the same sinewave signal of the previous simulation. In this case, the spectrum of the excitation voltage and the current through the contact are the ones shown in Fig.(5.6) and Fig.(5.7).

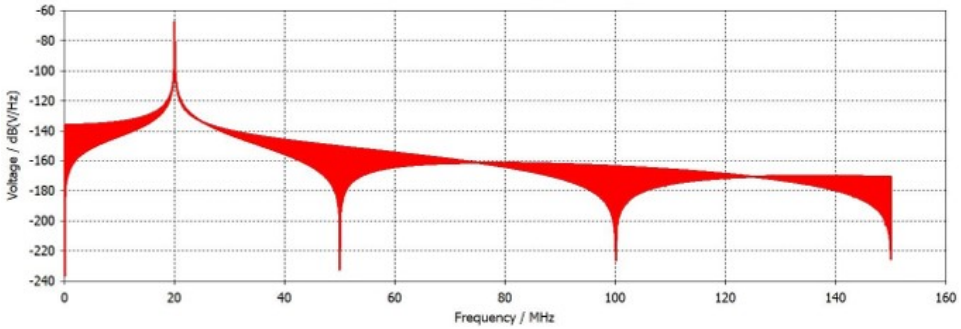

Figure 5.6. Spectrum of the excitation voltage used for the simulation of the setup in figure (5.4)

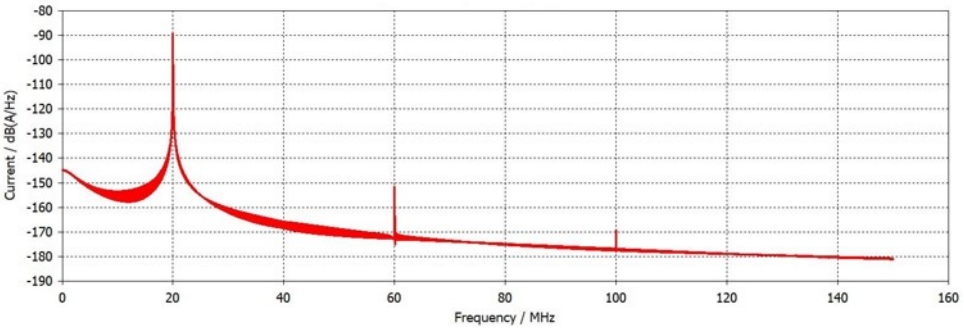

Figure 5.7. Spectrum of the current through the contact of the setup in figure (5.4)

In this case, in addition to the fundamental frequency component at $f = 20\text{MHz}$, we can notice in the current spectrum, the presence of other two frequency components at $f_1 = 3 \times f = 60\text{MHz}$ and $f_2 = 5 \times f = 100\text{MHz}$.

5.2 Implementation of the model in CST

After having shown the presence of PIM products thanks to the above preliminary simulations, we proceeded with the implementation of the model explained in the *Test 4* and reported in figure 4.11 in *CST Microwave Studio*. The complete *3D* model is reported in Fig.(5.8).

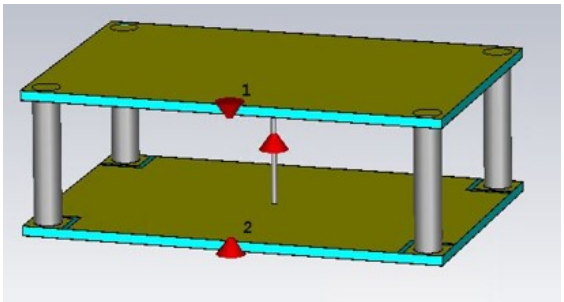

Figure 5.8. Complete *3D* model of the jig explained in *Test 4*

As depicted in the figure, the model consists of two PCBs separated by four cylinders of steel in the corners, with a steel wire in the middle connecting the two inner sides of the PCBs. Each PCB is composed of two films of copper (the yellow ones in figure) with a dielectric layer in the middle (the one in light blue). The reason of the presence of the copper film outside is that this latter acts as a ground plane for the whole system. Indeed, the four cylinders in the corners does not have only a support function, but they are used also for connecting the two external copper layers, making a single ground plane. It is important to notice that, as done for the real jig in *Test 4*, the inner layers of copper were cut near the corners in order to isolate these latter, and in this way the ground plane, from the rest of inner layers. The main difference between this model and the one used in the preliminary simulations above is the presence of a third discrete port in the middle of the steel wire. Indeed, unlike the case before in which only half model was built, in this case we realized the complete jig and this new port allows to insert the equivalent circuit model which is able to reproduce the PIM products. The choice of where to place the third port was a critical point. At the beginning this latter was placed at the

extremity of the wire, between the wire and the inner side of the copper layer of one PCB. But, after having performed some simulations and checked that the results are about the same, we decided to move it in the middle of the wire for reasons of symmetry of the model. The other two ports, are placed as before, between the edges of the outside copper layers (ground plane) and the inner ones. Once completed the realization of the model, the boundary conditions and the frequency range have to be set. The boundary conditions were setted *"Open"* and the frequency range was setted from 0.1MHz to 150MHz. Also in this case, the *"Transient solver"* was used in order to simulate the *3D* model. Once characterized the model from the *3D* point of view, we moved in the *Schematic* mode. In order to insert properly the equivalent circuit model developed, we needed to change the normal view mode of the ports to differential one. The whole schematic model is reported in Fig.(5.9).

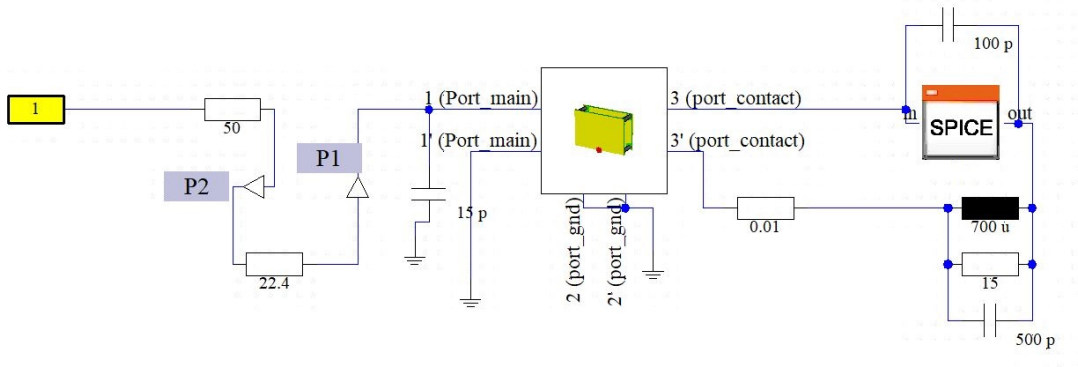

Figure 5.9. Schematic view of the model

Let's analyze in detail the above schematic circuit. *Port 1* is connected to a source generator (in yellow in the figure) through two resistances in series. The first one, equal to 50Ω is connected to the input source in order to replicate the output impedance of the signal generator used in the laboratory for the measurements. The second one, with a value of 22.4Ω, is the resistor we put in all developed setups between the signal generator and the real jig. In addition to these resistances, a shunt capacitor of 15pF is connected to model the input capacitance of the used oscilloscope. Before and after the 22Ω resistor, two probes, respectively P_2 and P_1, are inserted in order to monitor the current and the voltage at the source and on the contact. The other pin of *Port 1* is connected to ground. Both pins of *Port 2* are connected to ground. The most important port for the purposes of this thesis is the third one. Indeed, between the pins of *Port 3* is connected the circuit model

developed. In this case, in order to obtain the best fit between the waveforms obtained from measurements and simulations, we chose the following parameters:

Parameter	Value
R_C	0.01Ω
C_1	100pF
R_2	15Ω
C_2	500pF
L_2	700μH

Also in this case, the wanted non linear behaviour is given by the *SPICE* block that is the controlled-voltage current generator. This latter was setted using the coefficients obtained by fitting the measured characteristic with a polynomial of the 7^{th} order. The resulting current equation as a function of the applied voltage is:

$$i(v) = 0.0007v^7 - 0.0004v^6 - 0.026v^5 + 0.0017v^4 + 0.0104v^3 - 0.0015v^2 + 0.0198v \quad (5.1)$$

Also in this case, being the I-V characteristic of the real contact an odd function, the even terms of the equation are very close to zero. The implementation of the *SPICE* block is reported in Fig.(5.10).

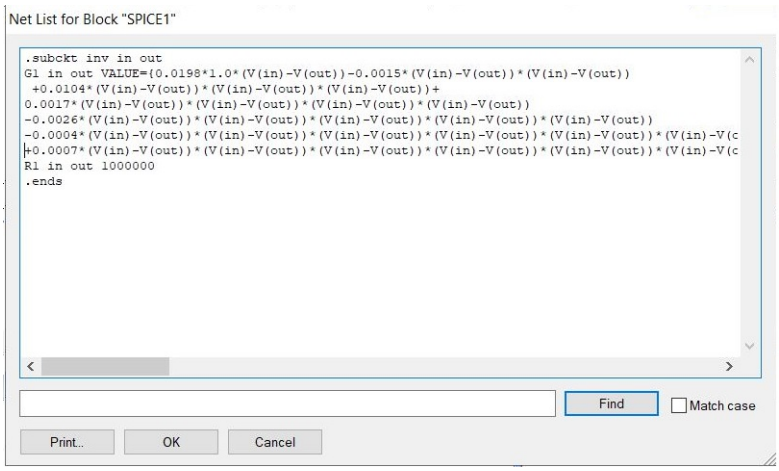

Figure 5.10. Implementation of the *SPICE* block in the schematic of figure (5.9)

Furthermore, as we can notice in Fig.(5.10), the *SPICE* block also included a shunt resistance of 1MΩ in order to avoid numerical instability in the simulation.

5.3 Simulation results

In order to validate the model in a proper way, we did not analyze only the PIM, but we compared also the I_x-V_x characteristic of the jig built in *Test 4* and the model implemented on *CST* for several values of frequency of the input signal. The above schematic circuit was simulated using a *Transient* task in which a triangular waveform is used as input signal. The resulting I_x-V_x characteristics obtained from simulations and the measured ones are compared in figures from (5.11) to (5.19), for the following values of frequency (50Hz, 500Hz, 1kHz, 5kHz, 10kHz, 50kHz, 100kHz, 500kHz, 1MHz).

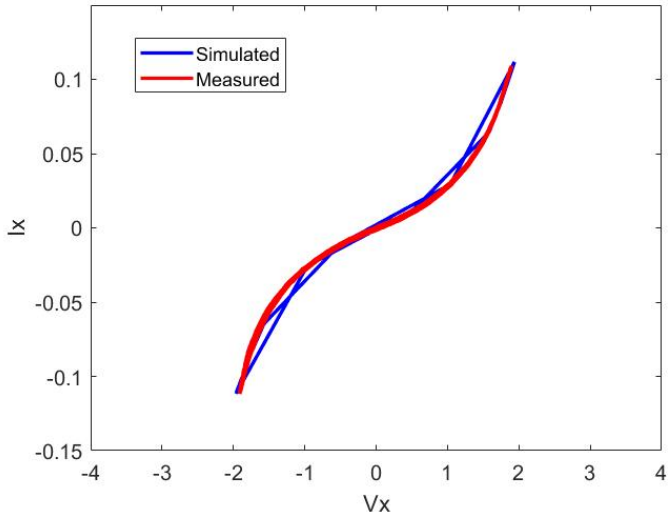

Figure 5.11. Comparison between the I_x-V_x characteristics obtained from simulation (blue line) and the measured one (red line) for an input signal with frequency $f = 50\text{Hz}$

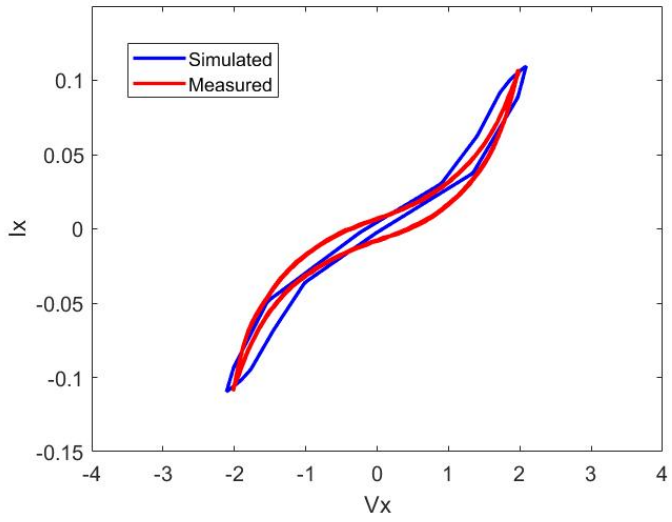

Figure 5.12. Comparison between the I_x-V_x characteristics obtained from simulation (blue line) and the measured one (red line) for an input signal with frequency $f = 500\text{Hz}$

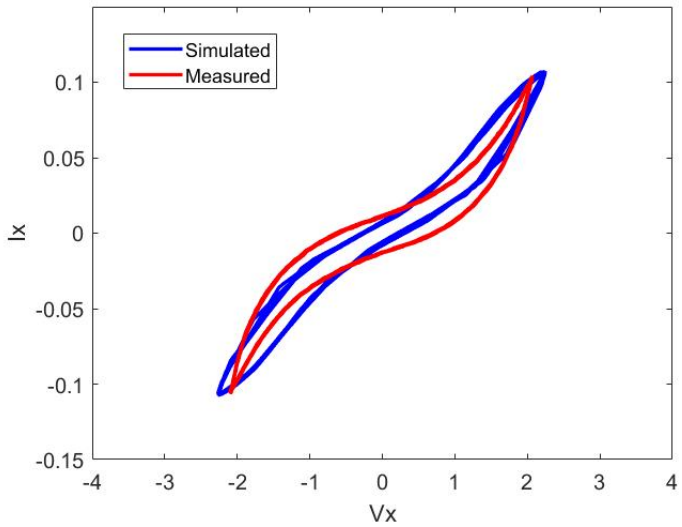

Figure 5.13. Comparison between the I_x-V_x characteristics obtained from simulation (blue line) and the measured one (red line) for an input signal with frequency $f = 1\text{kHz}$

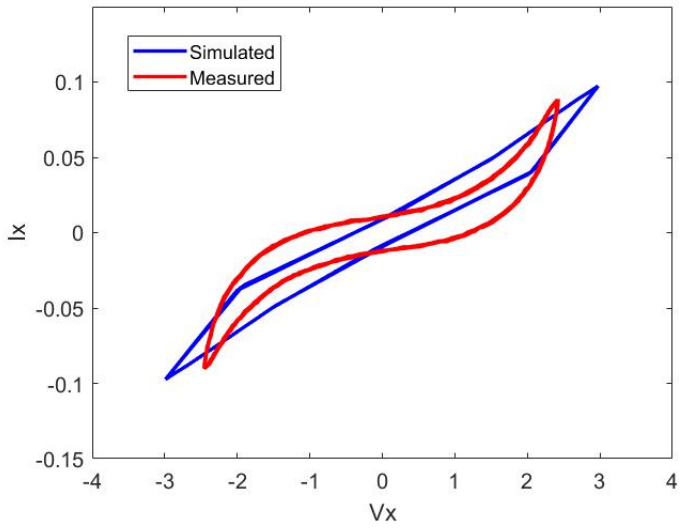

Figure 5.14. Comparison between the I_x-V_x characteristics obtained from simulation (blue line) and the measured one (red line) for an input signal with frequency $f = 5$kHz

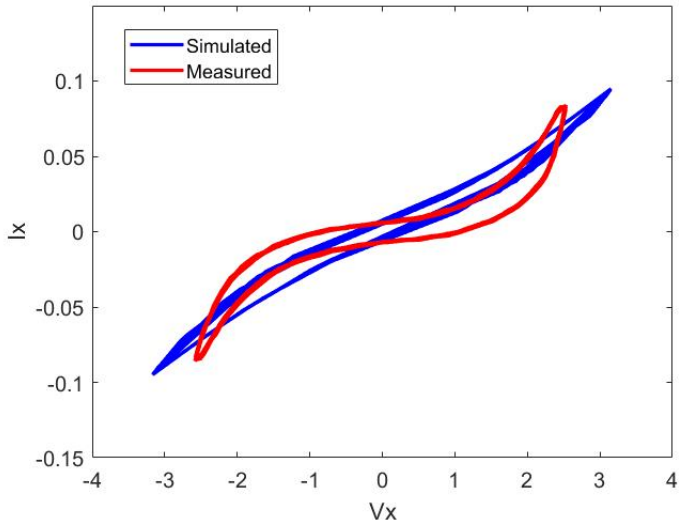

Figure 5.15. Comparison between the I_x-V_x characteristics obtained from simulation (blue line) and the measured one (red line) for an input signal with frequency $f = 10$kHz

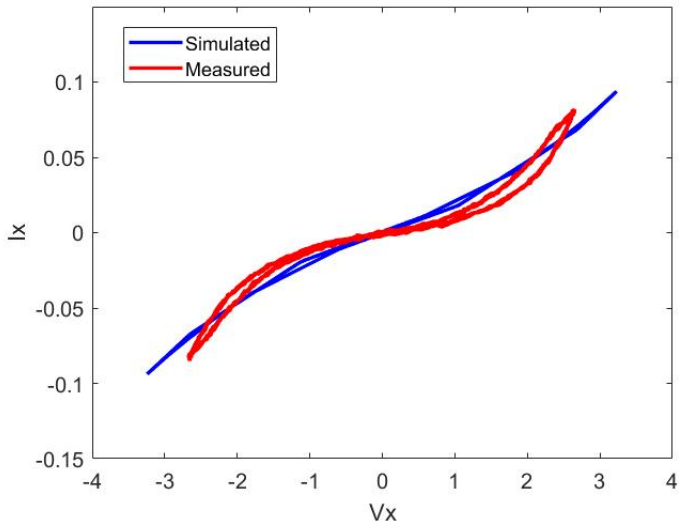

Figure 5.16. Comparison between the I_x-V_x characteristics obtained from simulation (blue line) and the measured one (red line) for an input signal with frequency $f = 50$kHz

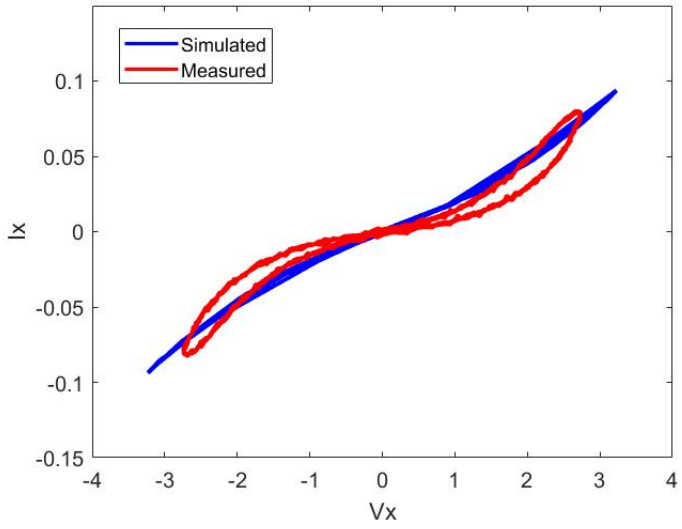

Figure 5.17. Comparison between the I_x-V_x characteristics obtained from simulation (blue line) and the measured one (red line) for an input signal with frequency $f = 100$kHz

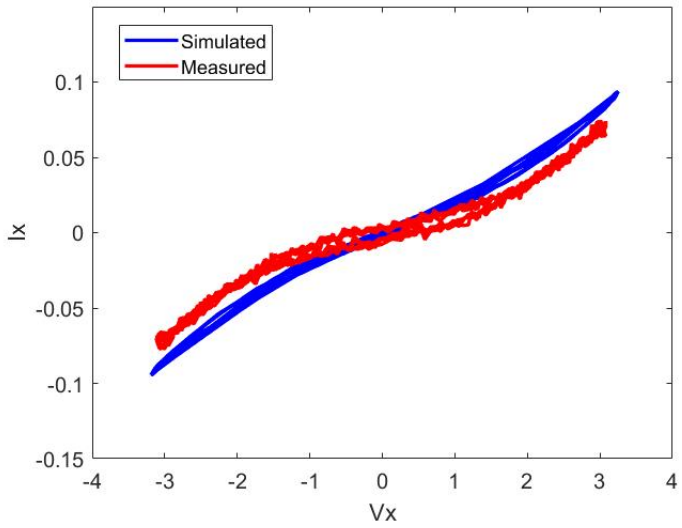

Figure 5.18. Comparison between the I_x-V_x characteristics obtained from simulation (blue line) and the measured one (red line) for an input signal with frequency $f = 500\text{kHz}$

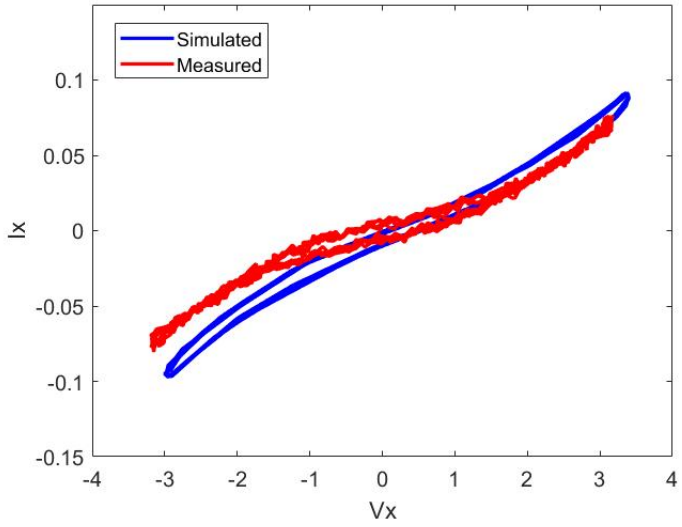

Figure 5.19. Comparison between the I_x-V_x characteristics obtained from simulation (blue line) and the measured one (red line) for an input signal with frequency $f = 1\text{MHz}$

As we can notice from the plots, the developed model results more accurate for low frequencies with respect to higher ones. Furthermore, to make a more accurate analysis, we compared also the waveforms of voltage and current predicted by our model with the measured ones for the same values of input signal frequency considered before. The resulting voltage waveforms are reported in the figures from (5.20) to (5.28).

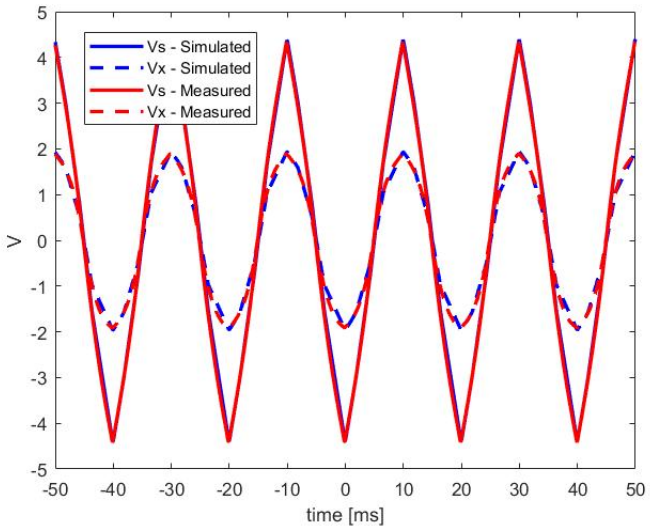

Figure 5.20. Comparison between the voltage waveforms of source V_s (solid lines) and across the contact V_x (dashed lines) obtained from simulations (blue lines) and the measured ones (red lines) for an input signal with frequency $f = 50$Hz

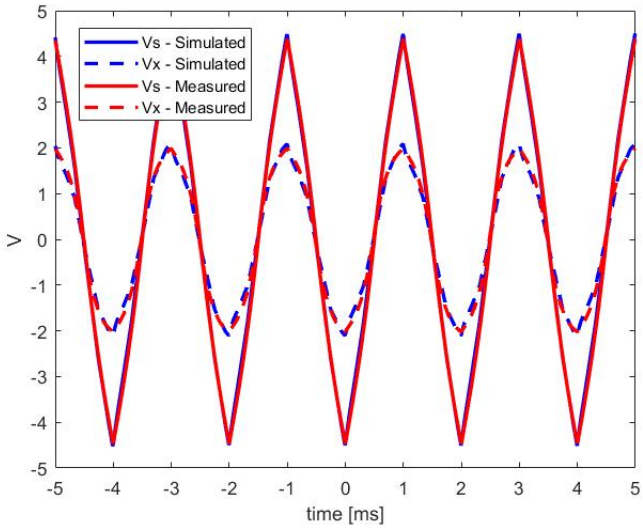

Figure 5.21. Comparison between the voltage waveforms of source V_s (solid lines) and across the contact V_x (dashed lines) obtained from simulations (blue lines) and the measured ones (red lines) for an input signal with frequency $f = 500$Hz

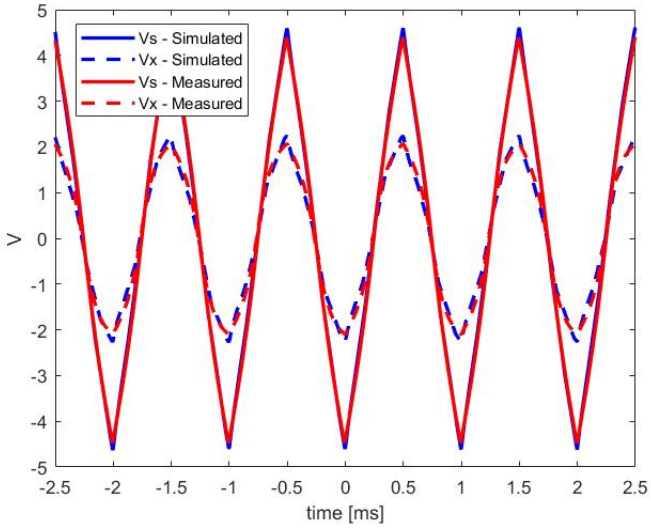

Figure 5.22. Comparison between the voltage waveforms of source V_s (solid lines) and across the contact V_x (dashed lines) obtained from simulations (blue lines) and the measured ones (red lines) for an input signal with frequency $f = 1$kHz

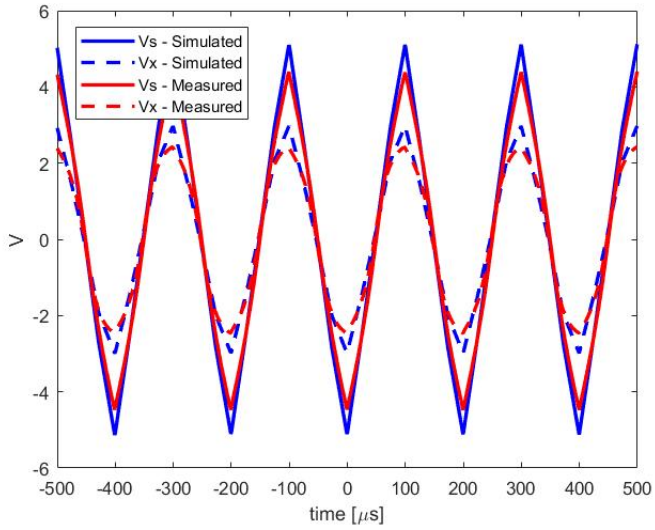

Figure 5.23. Comparison between the voltage waveforms of source V_s (solid lines) and across the contact V_x (dashed lines) obtained from simulations (blue lines) and the measured ones (red lines) for an input signal with frequency $f = 5$kHz

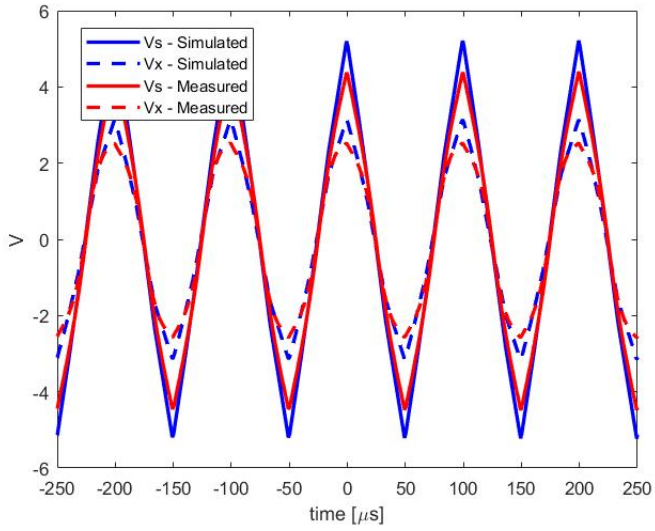

Figure 5.24. Comparison between the voltage waveforms of source V_s (solid lines) and across the contact V_x (dashed lines) obtained from simulations (blue lines) and the measured ones (red lines) for an input signal with frequency $f = 10$kHz

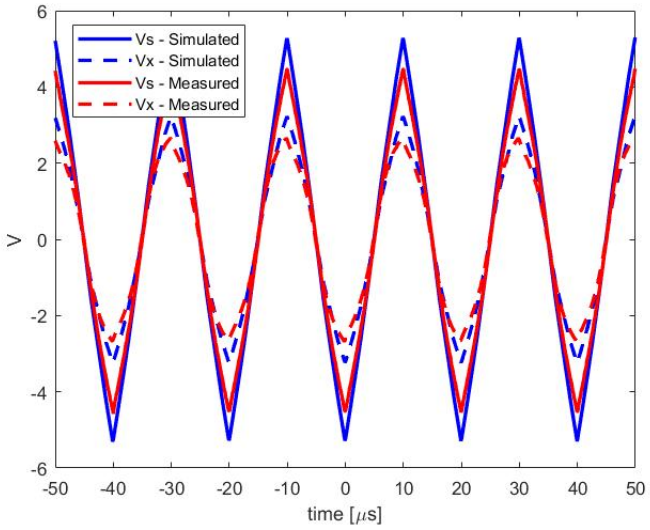

Figure 5.25. Comparison between the voltage waveforms of source V_s (solid lines) and across the contact V_x (dashed lines) obtained from simulations (blue lines) and the measured ones (red lines) for an input signal with frequency $f = 50$kHz

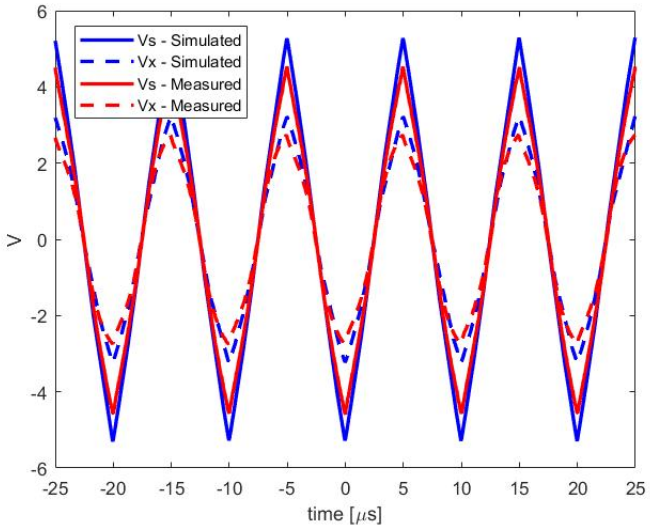

Figure 5.26. Comparison between the voltage waveforms of source V_s (solid lines) and across the contact V_x (dashed lines) obtained from simulations (blue lines) and the measured ones (red lines) for an input signal with frequency $f = 100$kHz

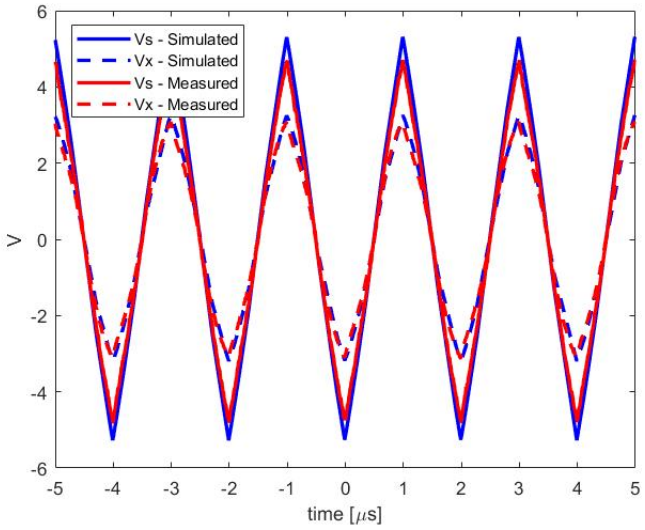

Figure 5.27. Comparison between the voltage waveforms of source V_s (solid lines) and across the contact V_x (dashed lines) obtained from simulations (blue lines) and the measured ones (red lines) for an input signal with frequency $f = 500$kHz

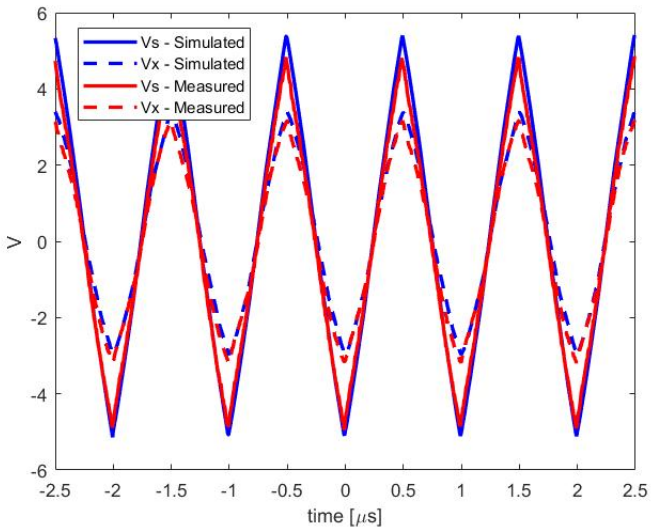

Figure 5.28. Comparison between the voltage waveforms of source V_s (solid lines) and across the contact V_x (dashed lines) obtained from simulations (blue lines) and the measured ones (red lines) for an input signal with frequency $f = 1$MHz

In the above plots, are reported the comparisons between the voltage waveforms obtained from simulations, with the blue lines, and the measured ones, with red lines, of two different voltages for several values of input signal frequency:

- The voltage on the source V_s (solid lines) through the probe P_2 in the schematic circuit reported in figure (5.9)
- The contact voltage V_x (dashed lines) through the probe P_1 of the same schematic circuit

Also for the waveforms of the current through the contact we proceeded in the same way, comparing the ones obtained from simulations with the measured ones for the same values of the input signal frequency considered before. The resulting waveforms of the current I_x are reported in figures from (5.29) to (5.37).

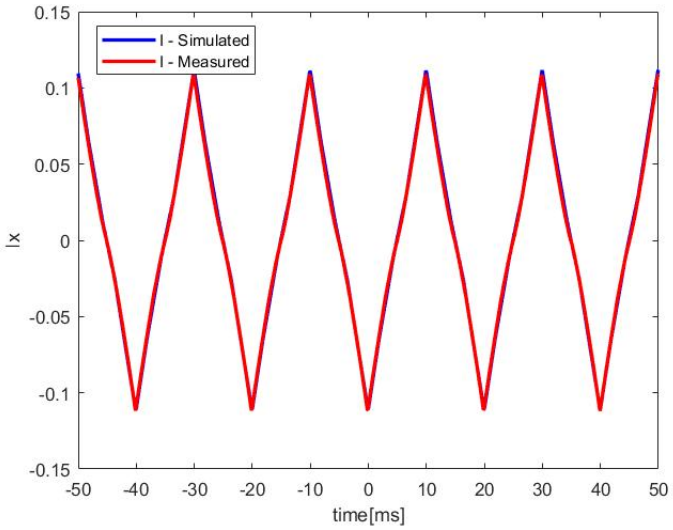

Figure 5.29. Comparison between the current waveforms obtained from simulation (blue line) and the measured one (red line) for an input signal with frequency $f = 50\text{Hz}$

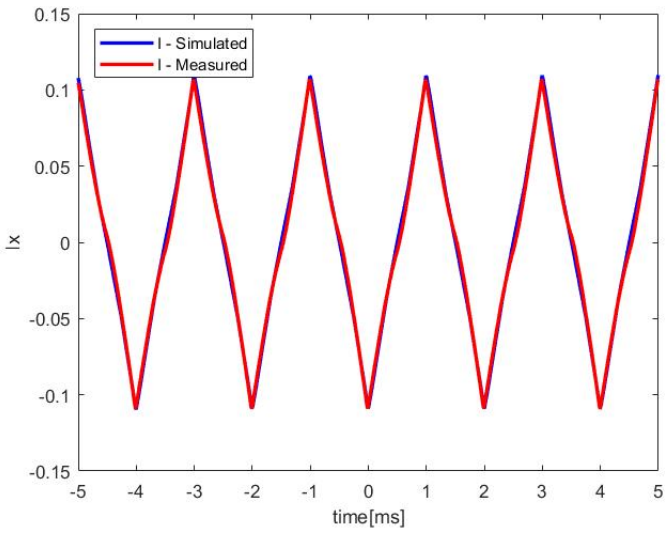

Figure 5.30. Comparison between the current waveforms obtained from simulation (blue line) and the measured one (red line) for an input signal with frequency $f = 500\text{Hz}$

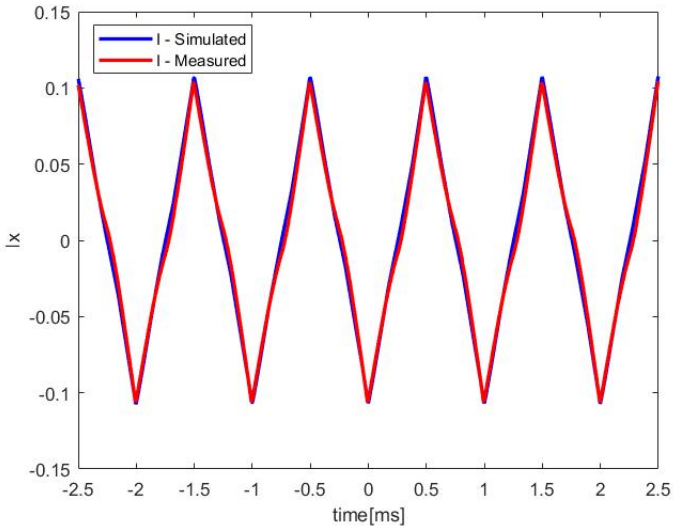

Figure 5.31. Comparison between the current waveforms obtained from simulation (blue line) and the measured one (red line) for an input signal with frequency $f = 1\text{kHz}$

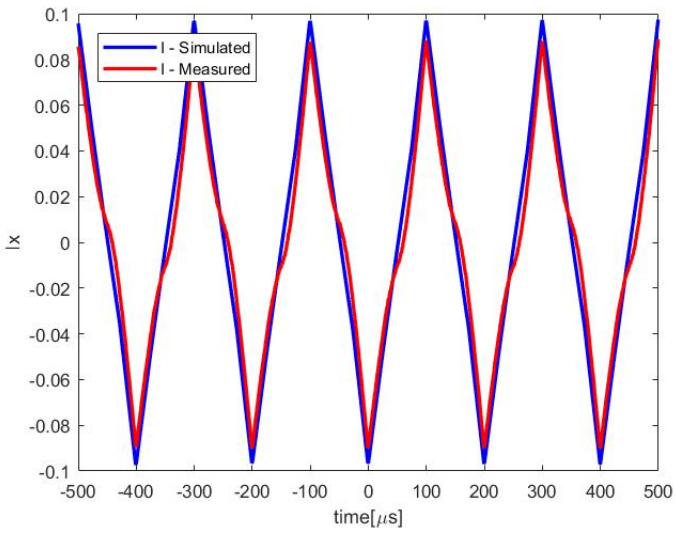

Figure 5.32. Comparison between the current waveforms obtained from simulation (blue line) and the measured one (red line) for an input signal with frequency $f = 5\text{kHz}$

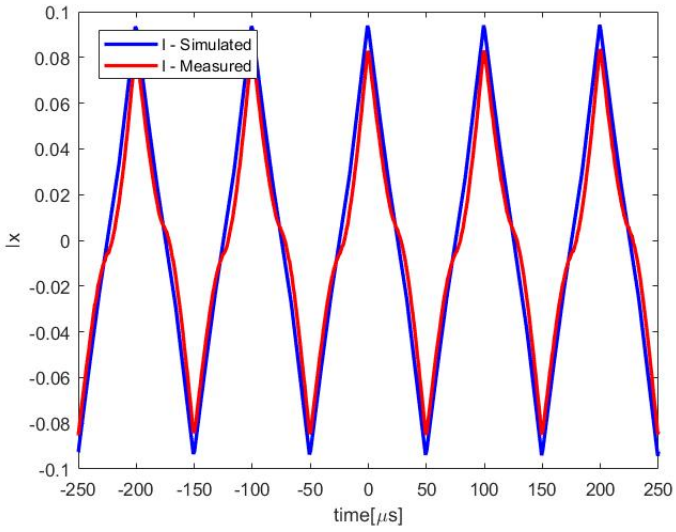

Figure 5.33. Comparison between the current waveforms obtained from simulation (blue line) and the measured one (red line) for an input signal with frequency $f = 10\text{kHz}$

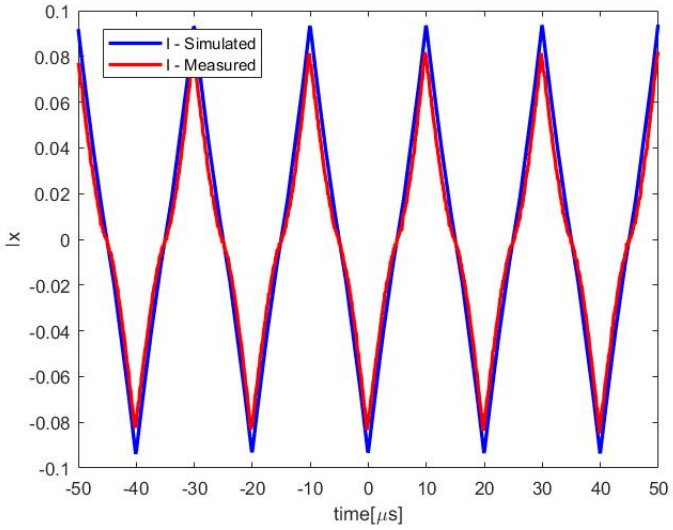

Figure 5.34. Comparison between the current waveforms obtained from simulation (blue line) and the measured one (red line) for an input signal with frequency $f = 50\text{kHz}$

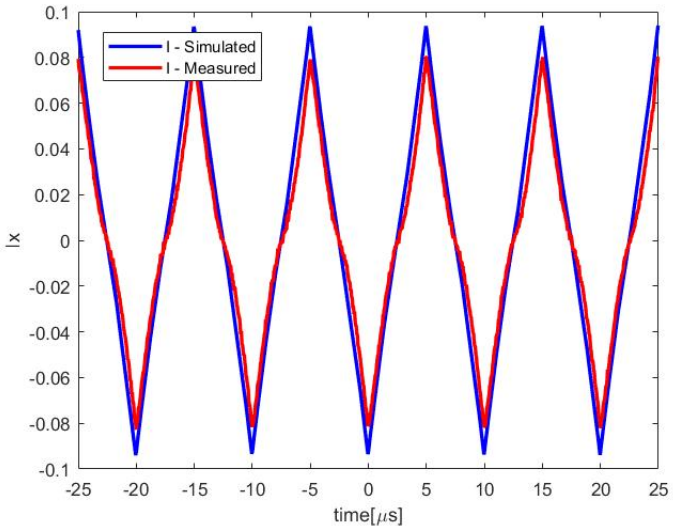

Figure 5.35. Comparison between the current waveforms obtained from simulation (blue line) and the measured one (red line) for an input signal with frequency $f = 100\text{kHz}$

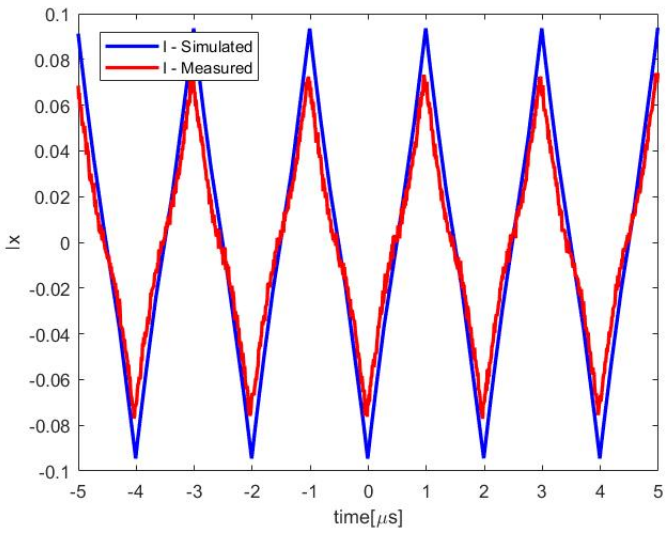

Figure 5.36. Comparison between the current waveforms obtained from simulation (blue line) and the measured one (red line) for an input signal with frequency $f = 500\text{kHz}$

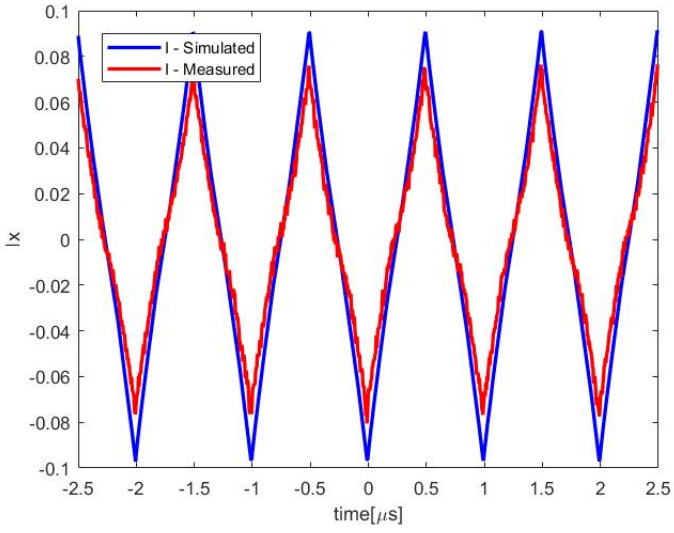

Figure 5.37. Comparison between the current waveforms obtained from simulation (blue line) and the measured one (red line) for an input signal with frequency $f = 1\text{MHz}$

Even if the model, looking at the I_x-V_x characteristics previously reported, results more accurate for low frequencies with respect to higher ones, we can notice from the plots above of the voltage and current waveforms, that this large error in the I_x-V_x curve is not reflected in a significant difference in the time domain waveforms. After having compared the voltage and current waveforms and having found that the developed model on *CST* and the experimental one agree, the last and most important step was analyze the PIM products in the output spectrum. In order to do this and make a comparison with the spectrum obtained from the measurements, we decided to excite the system with a sinusoidal waveform with the same frequency of the one used above $f = 1$MHz. Looking at the spectrum of the voltage on the contact (probe P_1), as done for the experimental model in the previous chapter, we can notice in Fig.(5.38) the presence, in addition to the fundamental frequency component, of PIM products at frequencies which are multiple of the fundamental one.

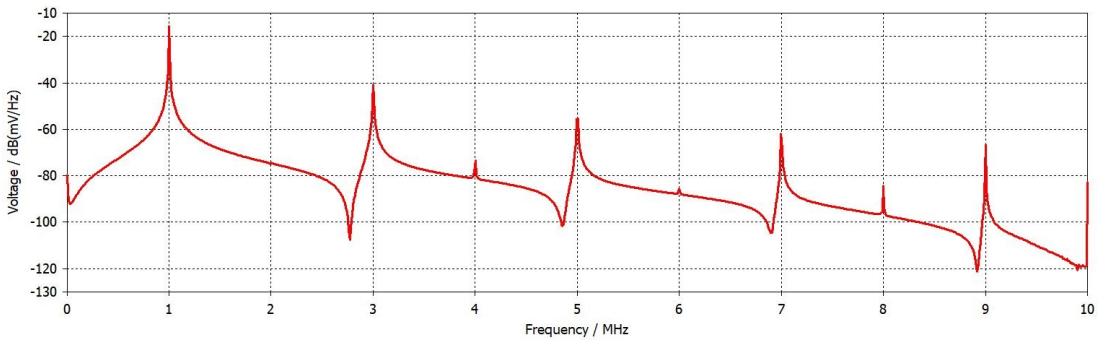

Figure 5.38. Spectrum of the voltage on the contact (probe P_1 of the schematic in figure (5.9)) obtained from simulations

The above voltage spectrum is compared with the one obtained from measurements thanks to the spectrum analyzer. Both spectra, respectively the one obtained from measurements and the simulated one, are reported in Fig.(5.39) and Fig.(5.40).

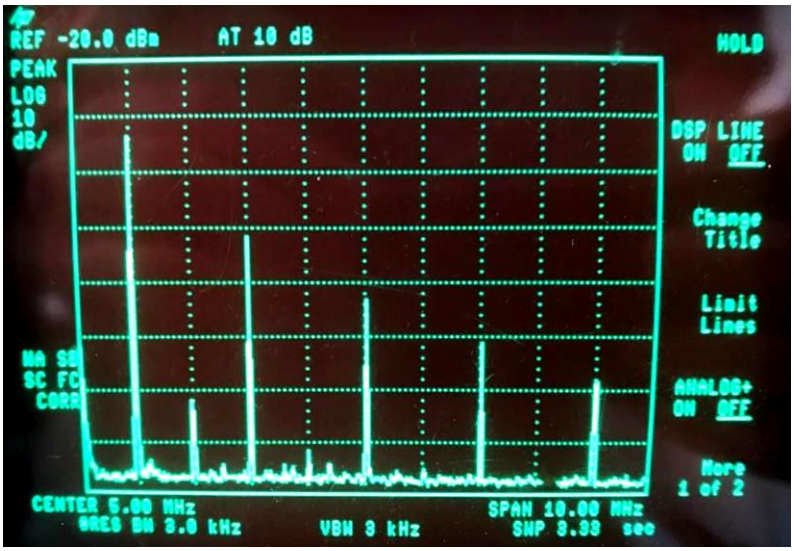

Figure 5.39. Spectrum of the voltage on the contact obtained from measurements

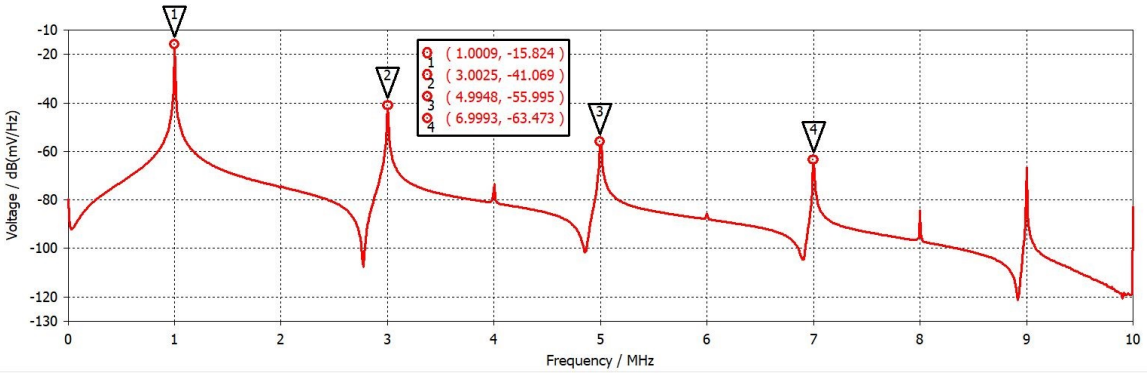

Figure 5.40. Spectrum of the voltage on the contact obtained from simulation

The two spectra of the voltage on the contact result slightly different. This is due to the low accuracy and reliability of the built test jig. The last step was to compare the voltage spectra on the contact in the case of two input signals with close frequencies, in order to compare the PIM products. In this case, the system was excited with two sinewave signals with frequencies $f_1 = 1$MHz and $f_2 = 1.5$MHz and the *Schematic* circuit was modified as shown in Fig.(5.41).

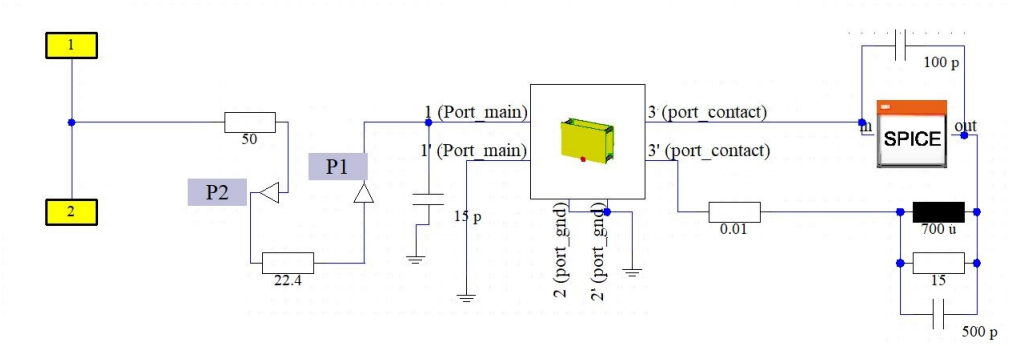

Figure 5.41. Schematic view of the model in case of two input signals

The only difference with the previous *Schematic* circuit is represented by the presence of a second port as source. The circuit in Fig.(5.41) was simulated in the same conditions of the previous one. The resulting spectrum of the voltage on the contact (always using probe P_1), together with the one obtained from measurements in the previous chapter and shown in Fig.(5.42), is reported in Fig.(5.43).

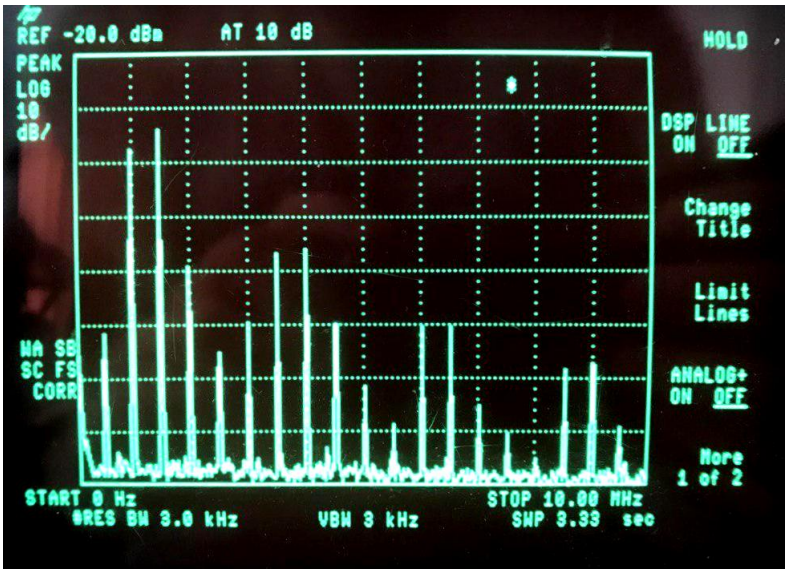

Figure 5.42. Spectrum of the voltage on the contact obtained from measurements in case of two input signals

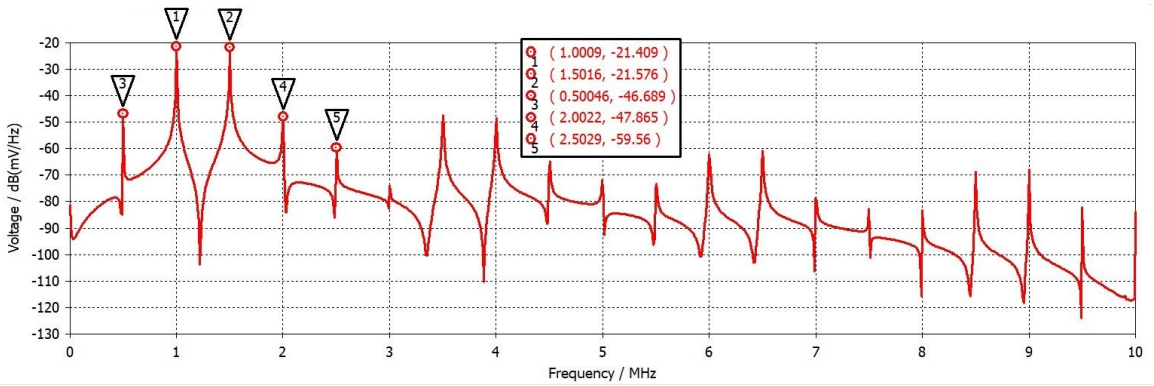

Figure 5.43. Spectrum of the voltage on the contact obtained from simulation

Also in this case, as we expected, there is a small difference between the reported spectra due to the same issues cited before.

Chapter 6

Conclusions and future works

In order to study and analyze the arise of PIM frequencies in communication systems, since these latter are due to non ideal metal-metal contacts in the systems, an equivalent circuit model able to explain and characterize the non linear behaviour of such a junction is needed. To accomplish this, two different approaches have been considered: a physical-based model and a behavioural-based one. Although a model based on the first approach could be very useful, providing a general model based on mathematical equations, on the other hand, such an approach may leads to a not accurate modelling scheme due to the inherent inexact and complex characteristic of non ideal contacts. Furthermore, this kind of model based on a physical approach is even more complex due to the multitude of microscopic effects that may be involved depending on the structure and materials of the considered metal-metal contact. For these reasons a behavioural-based approach became necessary. Thanks to this latter, it was possible to develop an equivalent circuit model which is able to fully characterize the considered contact. Thereafter, the model was validated through simulations performed using a full-wave solver (*CST Microwave Studio*). The main issue related to this approach is due to the reliability and the stability of the test jigs. Future works could be focused on the improvement of the accuracy of the developed model, like the introduction of frequency dependent components or the development of a circuit model of higher order, and on the investigation of the behaviour of the model at higher frequencies.

Bibliography

[1] Clarence D. Bond, Charles S. Guenzer and Carmine A. Carosella, *"Intermodulation generation by electron tunneling through aluminium-oxide films"*, Proceedings of the IEEE, vol.67, no.12, 1979

[2] Carlos Vicente, Hans L. Hartnagel, *"Passive-Intermodulation analysis between rough rectangular waveguide flanges"*,IEEE transactions on microwave theory and techniques, vol.53, no.8, 2005

[3] J. R. Wilkerson, P. G. Lam, K. G. Gard and M. B. Steer *"Distributed passive intermodulation distortion on transmission lines"*,IEEE transactions on microwave theory and techniques, vol.59, no.5, 2011

[4] Lior Kogut, Izhak Etsion, *"A finite element based elastic-plastic model for the contact of rough surfaces"*,Tribology Transactions, vol.46, 2003

[5] J. A. Greenwood, J. B. P. Williamson, *"Contact of nominally flat surfaces"*,Proceedings of the Royal Society of London, Series A, vol.295, 1966

[6] John G. Simmons, *"Generalized formula for the electric tunnel effect between similar electrodes separated by a thin insulating film"*, Journal of applied physics, vol.34, no.6, 1963

[7] H. Yang, H. Wen, Y. Qi and J. Fan, *"An equivalent circuit model to analyze passive intermodulation of loose contact coaxial connectors"*, IEEE transactions on electromagnetic compatibility, vol.60, no.5, 2018

[8] W. H. Higa, *"Spurious signal generated by electron tunneling on large reflector antennas"*, Proceedings of the IEEE, vol.63, no.2, 1975

[9] J. Russer, A. Ramachandran, A. Cangellaris and P. Russer, *"Phenomenological Modeling of Passive Intermodulation (PIM) due to Electron Tunneling at Metallic Contacts"*, 2006 IEEE MTT-S International Microwave Symposium Digest, 2006

[10] C. S. Guenzer, *"Comments on "Spurious signal generated by electron tunneling on large reflector antennas""*,Proceedings letters, 1975

[11] D. E. Zelenchuk, A. P. Shitvov, A. G. Schuchinsky and V. F. Fusco, *"Passive Intermodulation in Finite Lengths of Printed Microstrip Lines"*, IEEE transactions on microwave theory and techniques, vol.56, no.11, 2008

[12] T. Li, K. Zhang, J. Jiang, X. Ma, *"Passive intermodulation analysis of single contact junctions of wire mesh"*, J Comput Electron, 17, 2018